Topological Characterization and Investigation of Unconventional Superconducting Phases in Monolayer/Bilayer Models

Navketan Batra

A dissertation submitted for the partial fulfilment of BS-MS dual degree in Science

Supervised by
Dr. Sanjeev Kumar

April 2019

Certificate of Examination

This is to certify that the dissertation titled **Topological Characterization and Investigation of Unconventional Superconducting Phases in Monolayer/Bilayer Models** submitted by **Navketan Batra (Reg. No. MS14015)** for the partial fulfilment of BS-MS dual degree programme at Indian Institute of Science Education and Research, Mohali has been examined by the thesis committee duly appointed by the Institute. The committee finds the work done by the candidate satisfactory and recommends that the report be accepted.

Dr. Yogesh Singh | Dr. Goutam Sheet | Dr. Sanjeev Kumar (Supervisor)

Declaration

The work presented in this dissertation has been carried out by me under the guidance of Dr. Sanjeev Kumar at the Indian Institute of Science Education and Research, Mohali. This work has not been submitted in part or in full for a degree, a diploma, or a fellowship to any other university or institute. Whenever contributions of others are involved, every effort is made to indicate this clearly, with due acknowledgement of collaborative research and discussions. This thesis is a bonafide record of original work done by me and all sources listed within have been detailed in the bibliography.

Navketan Batra

(Candidate)

Dated: April 20, 2019

In my capacity as the supervisor of the candidate's project work, I certify that the above statements by the candidate are true to the best of my knowledge.

Dr. Sanjeev Kumar

(Supervisor)

Dated: April 20, 2019

Acknowledgements

I am deeply grateful to my advisor, Dr. Sanjeev Kumar - with the perfect combination of thoughtful criticism and constant encouragement, he has patiently led me through the journey. The door to his room is always open for discussion and he has always encouraged and presented me with the relevant literature and motivation to turn my ideas into something useful. Dr. Sanjeev has consistently allowed this work to be my own, and steered me in the right direction whenever he thought I needed it. I have also been very fortunate to closely collaborate with Swagatam Nayak. His never-let-go attitude challenged every aspect of our understanding and helped shape it correctly. With these two, I have left every conversation with a sense of wonder and a deeper understanding of my work.

Besides my advisor, I would like to thank Dr. Goutam Sheet for showering me with useful insights on topological insulators. The general article we wrote together for *Resonance* helped me immensely in this work. I also thank Arnob Mukherjee and Sudhanshu Chaurasia for helping me organise my code. By spending a whole year doing research, I have come to realise that modern research is, thankfully, not a socially isolated affair and I have benefited from the insights of many fellow 'researchers' of MS14 batch over short coffee breaks, movie nights and board game nights. I would like to particularly thank Shruti Maliakal, Swadheen Dubey, Jorawar Singh, Jaskaran, Samridhi Gambhir, Ayushi Singhania, and Swagatam Nayak for being around and providing me with a very stimulating environment. The five year long journey at IISER has transformed an eager physics enthusiast to an independent researcher - I will forever be grateful to the IISER Mohali community for providing me with all the necessary resources and amazing friends. Finally, for their unconditional love and support, I thank my mamma and papa, who valued my education more than anything else.

Abstract

In the first part of this dissertation, the effects of spin-dependent disorder on a conventional BCS superconductor is studied using Bogoliubov-de Gennes methods on a two dimensional attactive Hubbard model (AHM) and the results by Nanguneri et al., 2012 are reproduced. Next, by making use of a generalized definition of superconducting pairing order parameter mean-field calculations are performed on two dimensional Extended Attractive Hubbard Model (EAHM) and exotic unconventional SC phase diagrams are constructed. It is found that the nearest neighbour attractive interaction supports unconventional superconducting (SC) phases by allowing these phases to exist as a self-consistent broken symmetry solution at the mean-field level. These phases are then characterized based on their band structure in cylinder geometry and Chern indices.

In the second part, the monolayer SC model is generalized to a bilayer model by coupling a two-dimensional EAHM to a tight-binding model via inter-layer tunnelling and the proximity induced behaviour of SC order is explored with a focus on inducing topologically non-trivial SC character into the metallic layer. We show that interlayer tunnelling can drive changes in topology of the Bogoliubov quasiparticle bands leading to SC topological transitions. Finally, It is shown that these transitions can also be controlled by experimentally viable control parameters, the bandwidth of the metallic layer and the gate potential (Batra et al., 2019). The generic nature of the model used in this work suggests this can be applicable to a wide class of systems that invoke proximity effect. Our finding may open up a new route to discover topological superconductors which are considered to provide a fault-tolerant platform for topological quantum computing.

List of Figures

Contents

Chapter 1

Introduction

"Pick small problems - there is a jewel in every problem"
- Bogdan A. Bernevig, (2018)

1.1 Unconventional superconductivity

The Holy Grail of condensed matter physics, soon after the discovery of superconductors, has always been to understand the phenomenon of superconductivity. Although Bardeen, Cooper, and Schrieffer gave us an elegant microscopic theory of superconductivity (Ibach et al., 2009; Gennes, 1999), there still remains a large class of superconductors that is not understood microscopically (Monthoux et al., 2007; Cao et al., 2018; Aggarwal et al., 2016). This class of superconductors is known as *unconventional* superconductors[1]. The importance of such unconventional superconducting phases was immediately recognized soon after the discovery of materials which have normal-to-superconducting transition temperature, T_c well beyond the limits predicted by the BCS theory[2] (Chu et al., 1987). The reader should be careful here that having a higher T_c than predicted by the BCS theory is *not* a definition of unconventional superconductor! The unconventionality comes from the fact that even though the fundamental charge carriers in a superconductor are Cooper pairs, the Cooper pairing mechanism is not originated from the electron-phonon interaction. The pairing mechanism in an

[1] A more precise definition of unconventional superconductors will be given later in this section.

[2] From BCS theory the expectation was that the transition temperature, T_c would hardly overcome the barrier of $30K$! However, unconventional superconductors have been observed with T_c as high as 138 K at normal pressure and a record breaking T_c of 203 K, which was observed recently (2015) in H_2S, under extremely high pressure of about 150 gigapascals! See fig. 1.2.1.

unconventional superconductor therefore remains as an unsolved problem (Monthoux et al., 2007). Alongside, the paradigm of topological phases developed (Moore, 2010; Hasan et al., 2010; Shen, 2017) and soon it was realised that the theory that is applied to the vacuum of insulators, namely *topological insulators*, can be extended to superconductors as well (Qi et al., 2011). This led to another major theoretical prediction of the existence of Majorana fermions in topological superconductors having a strange property of non-abelian exchange statistics[3] (C. Nayak et al., 2008; Tsuei et al., 2000; Oreg et al., 2010; Nadj-Perge et al., 2008). In situations where the many body ground state wave function is a linear combination of states from a degenerate subspace, a pairwise exchange of the particle is non-abelian. In the case of non-abelian statistics, the exchange statistics is given by a multidimensional unitary matrix representation of the 2D braid group, and since it is non-abelian, the exchange of two particles is represented by their world lines as if they are being 'braided together'. These braiding operations, or particle exchange operations, have been shown to be useful for performing quantum computation (C. Nayak et al., 2008). The importance of this is that the principal obstacles on the road to quantum computing are noise and de-coherence which can be solved if we work with such states which are protected by some symmetry! All these potential applications suggest the importance and require deep understanding of unconventional superconductors. In a superconductor, the symmetries of the gap function $\Delta(\mathbf{k})$ encodes all the symmetry properties of the Cooper pair wavefunction (Sigrist et al., 1991; Tsuei et al., 2000; Mackenzie et al., 2003). BCS theory assumes the homogeneous and isotropic nature of the gap function $\Delta(\mathbf{k}) = \Delta_0$, whereas, from experiments it is confirmed that the gap function of an unconventional superconductor is not independent of the crystal momentum, $\mathbf{k}$. We can then characterise a superconductor by the symmetries of a Cooper pair wave function $\psi(\mathbf{k_1}, \mathbf{k_2}, s_1, s_2)$. In the absence of spin-orbit coupling, we can separate the spin and orbital parts of the wavefunction as,

$$\psi(\mathbf{k_1}, \mathbf{k_2}, s_1, s_2) = \phi(\mathbf{k_1}, \mathbf{k_2})\chi(s_1, s_2) \tag{1.1}$$

[3]Being a little more careful here - Majorana fermions are really fermions, as the name suggests, and therefore obey Fermi statistics. In condensed matter systems, there are (theoretically predicted) zero energy modes that follow non-abelian statistics. Particularly, in topological superconductors these modes are equal superposition of particle and hole which is why they are termed are Majorana particles; calling them Majorana 'modes' instead of 'fermions' would be adequate and unambiguous.

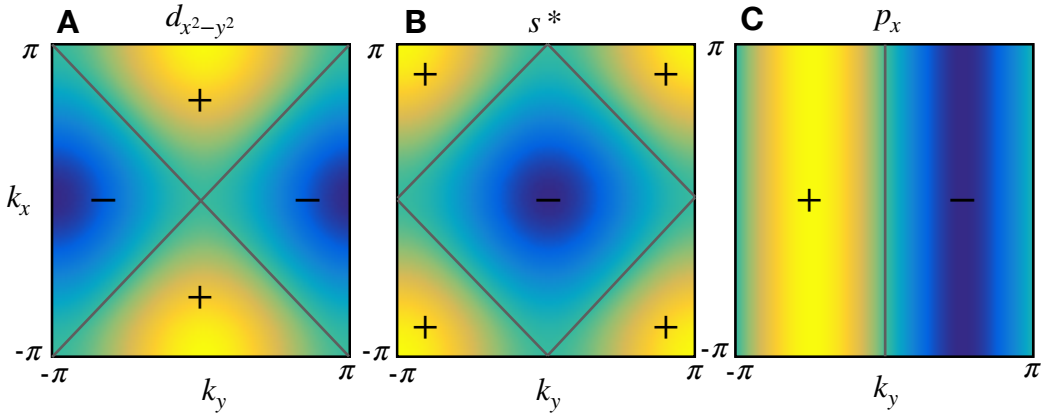

Figure 1.1.1: Figure shows the gap function $\Delta(\mathbf{k})$ in the Brillouin zone for (a) $d-$wave (b) extendend s, or $s*-$wave, and (c) p_x-wave unconventional superconductor.

A superconducting state can be of either total spin $S = 0$ (spin singlet) or $S = 1$ (spin triplet) depending on the spin wavefunction[4]. Due to Pauli's principle, the overall wavefunction of a Cooper pair has to be anti-symmetric under particle exchange, therefore, the *antisymmetric* spin-singlet state is accompanied by a *symmetric* orbital wave function (even parity) with orbital angular momentum $L = 0$ (known as $s-$wave), $L = 2$ (known as $d-$wave), and so on. The *symmetric* spin-triplet state is accompanied by an *antisymmetric* orbital wave function (odd parity) with orbital angular momentum $L = 1$ (known as $p-$wave), $L = 3$ (known as $f-$wave), and so on[5]. The conventional BCS superconductor is an $s-$wave superconductor because of its isotropic nature. In figure (1.1.1), the magnitude of the gap function, $|\Delta(\mathbf{k})|$, for various unconventional superconductors is shown. Notice their similarities to the atomic orbitals from which their names are borrowed. Note that for the conventional case, the gap function is going to be constant throughout the Brillouin zone. The constant phase of the gap function also reflects the fact that the local $U(1)$ gauge symmetry is broken and all the Cooper pairs are coherent. For the conventional $s-$wave superconductor no other symmetries are broken other than the $U(1)$ local gauge symmetry however, in the case of unconventional superconductors there are further symmetries that are broken, for example, in $d-$wave, additionally $\pi/2$ rotational symmetry is also broken - this broken symmetry aspect is also reflected in its gap function (Sigrist et al., 1991).

[4]This characterization of Cooper pairs in a superconductor leads to a spin-singlet or spin-triplet nomenclature which we also adopt in this work.

[5]This notion $s-, p-, d-, f-$wave is borrowed from their similarity to atomic orbital symmetries and carries no further meaning.

Unconventional superconductivity can therefore be defined, in terms of its gap function (Tsuei et al., 2000), by the relation,

$$\sum_{\mathbf{k}} \Delta(\mathbf{k}) = 0 \tag{1.2}$$

A property of $s-$wave superconductor is that the superconducting order is robust against reasonable amount of disorder - this is known as the Anderson's theorem. An immediate consequence of relation (1.2) is that Anderson's theorem does not apply to unconventional SC and the order parameter can be averaged to zero by sufficiently strong scattering. It is therefore not surprising that even though many unconventional superconductors have transition temperatures higher than conventional superconductors, it took a long time to discover unconventional superconductivity after the conventional superconductors were discovered (Mackenzie et al., 2003). Before closing this section, I would like to make a point that when high-T_c superconductivity was discovered in copper oxides (cuprates), it was realised that a quasi-two-dimensional structure is necessary for the existence of high-T_c superconductivity which is seen in the cuprates due to the planar CuO_2 network (G.-Y. Zhu et al., 2016; Zhang et al., 2010). Therefore, a two dimensional model, motivated by the high-T_c cuprate superconductors, has been chosen for this work.

1.2 Motivation and guiding problems

Superconductor, a new quantum state of matter, after being discovered came along with many challenges and exciting new possibilities (Cao et al., 2018; Aggarwal et al., 2016). The obvious one was macroscopic phase coherence that results in resistance-less electronic flow. The natural direction many scientists were attracted towards was to somehow enhance the transition temperature. This lead to the discovery of unconventional superconducting materials based on doped alloys see Fig. 1.2.1. These compounds are anti-ferromagnetic Mott insulators and miraculously become superconducting when appropriately doped. This transition from anti-ferromagnetism to superconductivity has posed many question that whether these two phases can coexist (Abram et al., 2013). Understanding this transition may also reveal whether Cooper pairing has anything to do with magnetism since both phenomena are a consequence of strong correlation (Chen et al., 2010). Motivated by this, we explore one such model with on-site re-

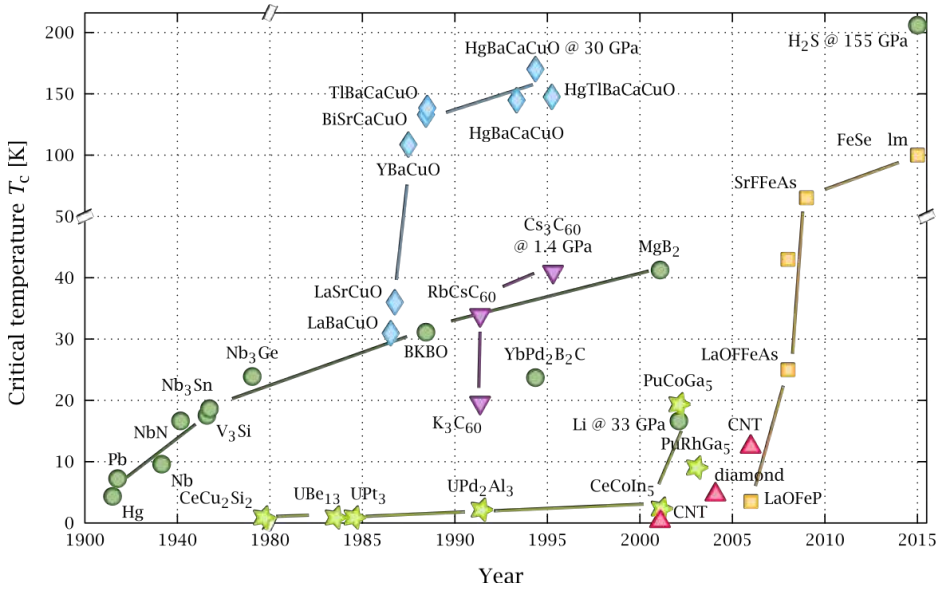

Figure 1.2.1: Timeline - discovery of superconductors with their respective critical temperature T_c. *Source: Wikipedia*

pulsive interaction and nearest neighbour attraction in order to incorporate competing anti-ferromagnetic and superconducting ground states. Incorporating disorder in superconducting systems has also been a rich area with many surprises (Dobrosavljevic et al., 2012). As discussed earlier, Anderson's work proved the robust nature of a three-dimensional conventional $s-$wave superconductor against disorder, the question remained what is the interplay of localization and superconductivity in two dimensions (Nanguneri et al., 2012; Kumar et al., 2015). A recent work also claims enhancement of normal-to-superconducting transition T_c due to disorder (Gastiasoro et al., 2018).

Superconductivity emerging in unexpected setting has also questioned our understanding time and again. Being known as *wonder material*, graphene fascinated physicists yet again by showing signatures of superconducting behaviour in twisted bilayer structures (Cao et al., 2018; Wu et al., 2018). With a twist angle of about 1.1° the electronic band structure exhibits flat bands near zero Fermi energy, resulting in correlated insulating states, which upon doping results in superconducting behaviour. Another such example is tip induced superconductivity (Aggarwal et al., 2016) - a mesoscopic point contact between silver (Ag) and a 3D Dirac semimetal (Cd_3As_2), neither of which is superconducting on its own, exhibit unconventional superconductivity. The common theme here is that bringing two layers close to one another alter the band structure. This

also motivate a question whether the band structure could be altered in such a way that it attains non-trivial topological character. Thus, a natural search for topological superconductivity began along the lines with spin-orbit coupling as the natural ingredient (Sau et al., 2010; Potter et al., 2011; X. Liu et al., 2014; Reeg et al., 2015; Alsharari et al., 2018). Due to a demanding platform (1D nanowires) for finding Majorana femions, recently, theoretical progress has also been made in generalizing the theory of conventional topological phases and bulk-boundary correspondence (Benalcazar et al., 2017b; Benalcazar et al., 2017a). These are known as Higher Order Topological Insulators (HOTI) and in general connect invariant calculations in the d dimensional bulk to the states in $d - m$ dimensional boundary. This way it may be possible to construct systems with Majorana bound states appearing as corner states. All in all, there are many unsolved problems in the field of superconductivity and there is still interesting physics in these systems that needs to be worked out. Before any of these questions can be tackled in its full glory, we need to understand superconducting behaviour in different settings. With this motivation, we work with a prototypical model for proximity induced superconductivity in a general setting with these broad questions in mind, and focus on inducing topologically non-trivial character in superconductors.

Chapter 2

Methodology

2.1 Bogoliubov-de Gennes formalism in tight binding model

For superconductors like high-temperature cuprates, the electronic band is quite narrow i.e., the orbitals have a small overlap between adjacent atoms. We therefore make use of the tight-binding Hamiltonian, which is either constructed from atomic orbitals or from Wannier orbitals, to study narrow band behaviours arising from electronic correlation effects (J.-X. Zhu, 2016). Bogoliubov-de Gennes (BdG) method relies on the assumption that there exists a well-defined quasiparticle excitation spectrum in a superconductor. Throughout this thesis, we assume this is true for unconventional superconductors also. We will later strengthen this argument by comparing the particle density of states (DOS) calculated within the BdG framework to the DOS experimentally measured using scanning-tunnelling-microscopy (STM). We start with a 2D square lattice with periodic (toric) boundaries and define a tight-binding extended Hubbard model on this lattice. The model Hamiltonian is as follows:

$$H = -\sum_{\langle i,j\rangle,\sigma} t(c^{\dagger}_{i\sigma}c_{j\sigma} + \text{h.c.}) - \sum_{i\sigma} \mu n_{i\sigma} - U\sum_{i} n_{i\uparrow}n_{i\downarrow} - V\sum_{\langle i,j\rangle} n_i n_j \tag{2.1}$$

The sum over the angular brackets $\langle\cdot\rangle$ represents those *unordered* pairs (i, j) which are nearest neighbours to each other on the lattice. The spin degree of freedom is represented by σ. The spin-full electronic creation (annihilation) operators are represented by $c_{i\sigma}(c^{\dagger}_{i\sigma})$ at site i. Correspondingly, $n_{i\sigma} = c^{\dagger}_{i\sigma}c_{i\sigma}$ is the electronic number operator

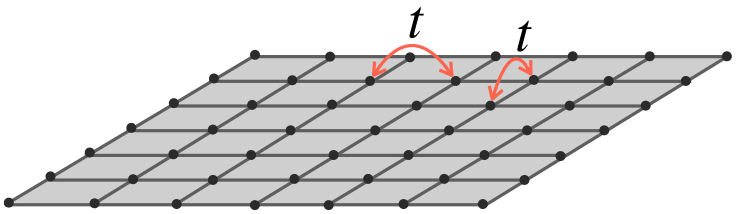

Figure 2.1.1: Pictorial representation of the two dimensional square lattice model.

and $n_i = \sum_\sigma n_{i\sigma}$ is the total electronic number operator at site i. The first term in the Hamiltonian, therefore, corresponds to the hopping potential t which represents the overlap between the nearest neighbour sites and is responsible for electronic kinetic part. The spin is preserved while the electron *hops* from one site to the other. Having this constraint is equivalent to setting the spin-orbit coupling set to zero. The third term is the chemical potential as we would like to work in a Grand Canonical ensemble. The final two terms are the interaction terms - the first of which is the on-site *effective* attractive potential for two electrons being at the same site. The last term is the *effective* attraction between two neighbouring electrons. These interaction terms, as we will see shall give rise to superconductivity. The on-site (nearest neighbour) interaction potential strength parameters, $U > 0$ ($V > 0$). It is also important to note here that this Hamiltonian is really an *effective* Hamiltonian, or a model Hamiltonian and the actual source of the interaction terms is unknown, unless we talk about the isotropic $s$wave SC order which is explained by the BCS theory. The nearest neighbour interaction term is responsible for the unconventional SC orders (Mackenzie et al., 2003; S. Nayak et al., 2018); although there are some theories, its complete origin is yet to be discovered.

2.1.1 Mean-field theory

Notice that the interaction terms in the Hamiltonian are the many body terms whereas others are single particle terms. Dealing with such many body interaction terms is a major issue in condensed matter as they increase the complexity of the problem significantly. We therefore make use of the *mean-field approximation* (Ashcroft et al., 1976; Simon, 2013).

Consider, two operators A and B. For small fluctuations $\delta A(\delta B)$, we may write the

operators as

$$\begin{aligned} A =& \langle A \rangle I + \delta A \\ B =& \langle B \rangle I + \delta B \end{aligned} \tag{2.2}$$

then the two operator interaction term can be approximated upto the first order of fluctuation as,

$$\begin{aligned} AB &\approx \langle A \rangle \langle B \rangle I + \langle B \rangle \delta A + \langle A \rangle \delta B \\ AB &\approx \langle B \rangle A + \langle A \rangle B - \langle A \rangle \langle B \rangle I \end{aligned} \tag{2.3}$$

where in the second step we make a substitution of $\delta A = A - \langle A \rangle$ and similarly for B. By making this approximation, we are left with only single operator terms and therefore, by making the mean-field approximation to our Hamiltonian all the interaction many body terms will reduce to effective single particle term which will be easy to work with.

Returning back to our Hamiltonian the interaction terms reduce to,

$$\begin{aligned} n_{i\sigma} n_{j\sigma'} \approx & \langle n_{i\sigma} \rangle n_{j\sigma'} + n_{i\sigma} \langle n_{j\sigma'} \rangle - \langle n_{i\sigma} \rangle \langle n_{j\sigma'} \rangle \\ & + \langle c^\dagger_{i\sigma} c^\dagger_{j\sigma'} \rangle c_{j\sigma'} c_{i\sigma} + c^\dagger_{i\sigma} c^\dagger_{j\sigma'} \langle c_{j\sigma'} c_{i\sigma} \rangle \\ & - |\langle c_{j\sigma'} c_{i\sigma} \rangle|^2 \end{aligned} \tag{2.4}$$

Notice, here we have decoupled the many body interaction terms in two different mean-field channels - $c^\dagger c c^\dagger c \to \langle c^\dagger c \rangle c^\dagger c$ which is the *density channel* and $c^\dagger c^\dagger c c \to \langle c^\dagger c^\dagger \rangle c c$ which is the called the *pairing channel*. We achieved this by just rearranging the fermionic operators appropriately. Since we do not expect the ground state to be a Fermi sea, we retain the anomalous pairing channel terms $\langle c_{i\downarrow} c_{j\uparrow} \rangle, \langle c_{i\uparrow} c_{j\downarrow} \rangle$ which shall go to zero in our calculations when the ground state will be Fermi sea like and will be non-zero otherwise. Here we also have assumed that $\langle c_\uparrow c_\uparrow \rangle$ ($\langle c_\downarrow c_\downarrow \rangle$) terms are zero! These terms correspond to $S_z \neq 0$ triplet superconducting pairs which we ignore by arguing that $S_z = 0$ triplet shall have same energy as other triplet components[1] since they differ only by a different choice of quantization axis[2]. Notice the terms from the

[1] This argument is valid only in the absence of Zeeman field.

[2] We will see that ignoring such terms simplifies our model by reducing the matrix into a block diagonal matrix

density channel only contribute to the chemical potential, known as the *Hartree Shift*, so we absorb those terms into the definition of the chemical potential itself. We finally arrive at the effective single particle Hamiltonian,

$$H = -\sum_{\langle i,j\rangle,\sigma} t[c^\dagger_{i\sigma}c_{j\sigma} + h.c.] - \sum_{i,\sigma}\mu c^\dagger_{i\sigma}c_{i\sigma} - U\sum_i[\Delta_i c^\dagger_{i\uparrow}c^\dagger_{i\downarrow} + h.c.] \\ - V\sum_{i,\delta}[\Delta^+_{i\delta}c^\dagger_{i\uparrow}c^\dagger_{i+\delta\downarrow} + \Delta^-_{i\delta}c^\dagger_{i-\delta\downarrow}c^\dagger_{i\uparrow} + h.c.] + E_{\text{const}} \tag{2.5}$$

Where we have introduced the pair expectation values in the ground state as, $\Delta_i = \langle c_{i\downarrow}c_{i\uparrow}\rangle$, $\Delta^+_{i\delta} = \langle c_{i+\delta\downarrow}c_{i\uparrow}\rangle$, and $\Delta^-_{i\delta} = \langle c_{i-\delta\downarrow}c_{i\uparrow}\rangle$ where δ denotes unit vectors +x and +y on the square lattice. Unlike conventional cases, we do not impose any symmetry[3] constraint on $\Delta^+_{i\delta}$ and $\Delta^-_{i,-\delta}$ and treat them as independent (S. Nayak et al., 2018).

$$\Delta^+_{i\delta} = \langle c_{i+\delta\downarrow}c_{i\uparrow}\rangle \tag{2.6}$$

$$\Delta^-_{i\delta} = \langle c_{i-\delta\downarrow}c_{i\uparrow}\rangle = \langle c_{i\downarrow}c_{i+\delta\uparrow}\rangle \tag{2.7}$$

where in the second definition, we have assumed uniformity of SC order along a bond $(i-\delta, i)$. This assumption needs to be relaxed if we allow for modulated SC orders. This pair expectation value encodes the information about the symmetry properties of a Cooper pair wavefunction. Any exchange of these electrons in a Cooper pair shall result in an overall minus sign if the spin part of the Cooper pair is a singlet and a plus $+$ sign if the spin part is a triplet. A slight rearrangement of the above definition would give us the conditions for spin-singlet and spin-triplet Cooper pairs as

$$\Delta^+_{i\delta} = \Delta^-_{i\delta} \qquad \text{spin-singlet} \tag{2.8}$$

$$\Delta^+_{i\delta} = -\Delta^-_{i\delta} \qquad \text{spin-triplet} \tag{2.9}$$

Not imposing any such properties on the definitions of pair-correlation functions is equivalent to allowing these phases to compete and show up only when it is energetically favourable. Motivated by this idea of working in a general class of pair correlation

[3]Note that when we talk about the symmetries of the correlation function, we mean it in a discrete sense - the correlation functions are only defined along a bond connecting two lattice sites *or* each lattice site has *four* such bonds. Therefore, there are only four such *axes* which we use to define our symmetry of the correlation functions on.

functions, we define various SC order parameters using these definitions as,

$$^{s\text{wave}}\Delta_i = \Delta_{ii} \tag{2.10}$$

$$^{s*\text{wave}}\Delta_i = [\Delta_{i,i+x} + \Delta_{i+x,i} + \Delta_{i,i+y} + \Delta_{i+y,i}]/4 \tag{2.11}$$

$$^{d\text{wave}}\Delta_i = [\Delta_{i,i+x} + \Delta_{i+x,i} - \Delta_{i,i+y} - \Delta_{i+y,i}]/4 \tag{2.12}$$

$$^{p_{x(y)}\text{wave}}\Delta_i = [\Delta_{i,i+x(y)} - \Delta_{i+x(y),i}]/2 \tag{2.13}$$

With the help of these definitions we will characterise the SC phase, based on which is non-zero, in the self-consistent calculations. We may also calculate their particle Density of States (DOS), to verify the SC phase with experimentally measured DOS. The purpose of this section was to arrive at the single particle mean field Hamiltonian which we will try to solve. In the next section, we apply Bogoliubov-de Gennes methods to this model Hamiltonian and set up a self-consistent calculation scheme.

2.1.2 Momentum space formalism

Working in periodic (toric) boundaries with uniform structure of hopping potential, such that translation invariance is preserved, has a nice advantage of going over to the Fourier space by transforming, $c_{i\sigma} = \frac{1}{\sqrt{N_s}} \sum_{\mathbf{k}} e^{-i\mathbf{k}\cdot\mathbf{r_i}} c_{\mathbf{k}\sigma}$, N_s being the total number of sites. We now make a Fourier transformation to the model mean-field Hamiltonian and get,

$$\mathcal{H}_{\text{eff}} = \sum_{\mathbf{k}} h(\mathbf{k}) + E_{\text{const}} \tag{2.14}$$

$$h(\mathbf{k}) = \sum_{\sigma} \xi^{\sigma}(\mathbf{k}) c^{\dagger}_{\mathbf{k}\sigma} c_{\mathbf{k}\sigma} + \left(\Delta^{\uparrow\downarrow}(\mathbf{k}) c^{\dagger}_{\mathbf{k}\uparrow} c^{\dagger}_{-\mathbf{k}\downarrow} + h.c. \right) \tag{2.15}$$

where we have defined,

$$\xi^{\sigma}(\mathbf{k}) = -2t(\cos k_x + \cos(k_y)) - \mu + \sigma B \tag{2.16}$$

$$\Delta^{\uparrow\downarrow}(\mathbf{k}) = -U\Delta_0 - V(e^{-ik_x}\Delta^{+}_{x} + e^{ik_x}\Delta^{-}_{x} + e^{-ik_y}\Delta^{+}_{y} + e^{ik_y}\Delta^{-}_{y}) \tag{2.17}$$

$$E_{\text{const}} = N_s(U|\Delta_0|^2 + V(|\Delta^{+}_{x}|^2 + |\Delta^{-}_{x}|^2 + |\Delta^{+}_{y}|^2 + |\Delta^{-}_{y})|^2) \tag{2.18}$$

We assume uniformity of the pair correlation functions, $\Delta^{\pm}_{i,\delta} = \langle c_{i\pm\delta\downarrow} c_{i\uparrow} \rangle \equiv \Delta^{\pm}_{\delta}$. Notice that we have also included Zeeman field term in Hamiltonian which will just relatively

shift the chemical potential. Here, $\sigma = \pm 1$ depicting the spins $\uparrow\downarrow$. It is worthwhile to note that because of the general structure of $\{\Delta_x^{\pm}, \Delta_y^{\pm}\}$, the symmetries of the SC gap function $\Delta^{\uparrow\downarrow}(\mathbf{k})$ are not fixed. Depending on the energy minimization, various symmetries may be imposed on the gap function that may lead to any kind of unconventional, or even conventional, SC order. We now calculate the commutation relations of the effective Hamiltonian with the fermionic creation and annihilation operators of electrons. We obtain,

$$[c_{k\uparrow}, \mathcal{H}_{\text{eff}}] = \xi^{\uparrow}(\mathbf{k}) c_{\mathbf{k}\uparrow} + \Delta^{\uparrow\downarrow}(\mathbf{k}) c^{\dagger}_{-\mathbf{k}\downarrow} \tag{2.19}$$

$$[c^{\dagger}_{-k\downarrow}, \mathcal{H}_{\text{eff}}] = -\xi^{\downarrow}(-\mathbf{k}) c^{\dagger}_{-\mathbf{k}\downarrow} + \Delta^{\uparrow\downarrow *}(\mathbf{k}) c_{\mathbf{k}\uparrow} \tag{2.20}$$

$$[c_{k\downarrow}, \mathcal{H}_{\text{eff}}] = \xi^{\downarrow}(\mathbf{k}) c_{\mathbf{k}\downarrow} - \Delta^{\uparrow\downarrow}(-\mathbf{k}) c^{\dagger}_{-\mathbf{k}\uparrow} \tag{2.21}$$

$$[c^{\dagger}_{-k\uparrow}, \mathcal{H}_{\text{eff}}] = -\xi^{\uparrow}(-\mathbf{k}) c^{\dagger}_{-\mathbf{k}\uparrow} - \Delta^{\uparrow\downarrow *}(-\mathbf{k}) c_{\mathbf{k}\downarrow} \tag{2.22}$$

One can now clearly see that these two equations are coupled to each other in an interesting way - operator $c_{\mathbf{k}\uparrow}$ couples to operator $c^{\dagger}_{-\mathbf{k}\downarrow}$ and operator $c_{\mathbf{k}\downarrow}$ couples to $c^{\dagger}_{-\mathbf{k}\uparrow}$. In fact, if we do a particle-hole transformation to down-spin electrons, the operator $c^{\dagger}_{-\mathbf{k}\downarrow}$ will exactly be the *annihilation* operator of a *hole* with down-spin. Notice that this coupling is due to the presence of finite SC order! So it is clear that due to the pairing correlation terms $\{\Delta\}$, equations (2.19-2.22) mix particles and holes. Recall these creation (annihilation) operators played a crucial role in setting up the structure of the states of a quantum harmonic oscillator. Similarly, the state label representing the number of particle excitation can be defined, however, these commutation relations do not satisfy the standard particle creation (annihilation) algebra, therefore, we do not expect the quasi-particles for the problem to be electron (or hole) like but something that is a superposition of these two. We therefore define new fermionic quasi-particle operators (J.-X. Zhu, 2016), $\gamma_{\mathbf{k}n}$ and $\gamma^{\dagger}_{\mathbf{k}n}$, that mix the electronic operators as,

$$c_{\mathbf{k}\sigma} = \sum_{n}{}' \left(u^{n}_{\mathbf{k}\sigma} \gamma_{\mathbf{k}n} - \sigma v^{n^*}_{\mathbf{k}\sigma} \gamma^{\dagger}_{-\mathbf{k}n} \right) \longleftrightarrow c^{\dagger}_{-\mathbf{k}\sigma} = \sum_{n}{}' \left(u^{n^*}_{-\mathbf{k}\sigma} \gamma^{\dagger}_{-\mathbf{k}n} - \sigma v^{n}_{-\mathbf{k}\sigma} \gamma_{\mathbf{k}n} \right) \tag{2.23}$$

with a constrain on $u^{n}_{\mathbf{k}\sigma}$ and $v^{n}_{\mathbf{k}\sigma}$ that the new operators γ and $\gamma^{\dagger}$ follow fermionic statistics i.e. $\{\gamma_{\mathbf{k}n}, \gamma^{\dagger}_{\mathbf{k}'m}\} = \delta_{nm}\delta_{\mathbf{k}\mathbf{k}'}$ and $\{\gamma_{\mathbf{k}n}, \gamma_{\mathbf{k}'m}\} = \{\gamma^{\dagger}_{\mathbf{k}n}, \gamma^{\dagger}_{\mathbf{k}'m}\} = 0$; this amounts to having $|u^{n}_{\mathbf{k}\sigma}|^2 + |v^{n}_{\mathbf{k}\sigma}|^2 = 1$ which is just a normalization condition. The symbol σ takes values ± 1 for $\uparrow\downarrow$ spin configuration and is introduced just for convenience. These new

operators are the quasi-particle excitations of the system and are called **Bogoliubov quasiparticles**. Notice the prime on the sum; this is a constraint to include only those n which will result in positive excitation energy as we have *doubled* the Hilbert space and would like to avoid over counting. We will come back to this in a short while. The Bogoliubov transformation is just an isomorphism of the canonical anticommutation algebra of the electronic operators in order to transform the commutation relations (2.19-2.22), to a simple standard form,

$$\begin{aligned}[\gamma_{\mathbf{k}n}, \mathcal{H}_{\text{eff}}] &= E_{\mathbf{k}n}\gamma_{\mathbf{k}n} \\ [\gamma^\dagger_{\mathbf{k}n}, \mathcal{H}_{\text{eff}}] &= -E_{\mathbf{k}n}\gamma^\dagger_{\mathbf{k}n}\end{aligned} \tag{2.24}$$

Now, using the transformation (2.23), the Hamiltonian is diagonalized in the following form,

$$\mathcal{H}_{\text{eff}} = \sum_{\mathbf{k},n} E_{\mathbf{k}n}\gamma^\dagger_{\mathbf{k}n}\gamma_{\mathbf{k}n} + E_{\text{const}} \tag{2.25}$$

Our motive was to have a description of superconductor very similar to the Harmonic Oscillator where the number states represent the number of excitation of the quasiparticles[4]. We can see that we have achieved such a form and moreover, we now know the excitation energy $E_{\mathbf{k}n}$ for every quasiparticle. But we are not done yet - we have to still know what the spectrum of the Bogoliubov transformation look like, in other words, what are the coefficients $\{u, v\}$ in (2.23). For this, assuming (2.25) we plug in the transformations (2.23) into the commutation relations (2.19-2.22) and by comparing the coefficients of $\gamma_{\mathbf{k}n}$, we obtain a set of four Bogoliubov-de Gennes equations:

$$u^n_{\mathbf{k}\uparrow}E_{\mathbf{k}n} = \xi^\uparrow(\mathbf{k})u^n_{\mathbf{k}\uparrow} + \Delta^{\uparrow\downarrow}(\mathbf{k})v^n_{-\mathbf{k}\downarrow} \tag{2.26}$$

$$v^n_{-\mathbf{k}\downarrow}E_{\mathbf{k}n} = -\xi^\downarrow(-\mathbf{k})v^n_{-\mathbf{k}\downarrow} + \Delta^{\uparrow\downarrow *}(\mathbf{k})u^n_{\mathbf{k}\uparrow} \tag{2.27}$$

$$u^n_{\mathbf{k}\downarrow}E_{\mathbf{k}n} = \xi^\downarrow(\mathbf{k})u^n_{\mathbf{k}\downarrow} + \Delta^{\uparrow\downarrow}(-\mathbf{k})v^n_{-\mathbf{k}\uparrow} \tag{2.28}$$

$$v^n_{-\mathbf{k}\uparrow}E_{\mathbf{k}n} = -\xi^\uparrow(-\mathbf{k})v^n_{-\mathbf{k}\uparrow} + \Delta^{\uparrow\downarrow *}(-\mathbf{k})u^n_{\mathbf{k}\downarrow} \tag{2.29}$$

[4] As already mentioned in the beginning of this chapter, all of this is possible assuming quasiparticle are well defined in a superconductor.

Likewise, we also obtain another set of four BdG equations by comparing coefficients of $\gamma^{\dagger}_{-\mathbf{k}n}$,

$$v^{n*}_{\mathbf{k}\uparrow}E_{-\mathbf{k}n} = -\xi^{\uparrow}(\mathbf{k})v^{n*}_{\mathbf{k}\uparrow} + \Delta^{\uparrow\downarrow}(\mathbf{k})u^{n*}_{-\mathbf{k}\downarrow} \tag{2.30}$$

$$u^{n*}_{-\mathbf{k}\downarrow}E_{-\mathbf{k}n} = \xi^{\downarrow}(-\mathbf{k})u^{n*}_{-\mathbf{k}\downarrow} + \Delta^{\uparrow\downarrow *}(\mathbf{k})v^{n*}_{\mathbf{k}\uparrow} \tag{2.31}$$

$$v^{n*}_{\mathbf{k}\downarrow}E_{-\mathbf{k}n} = -\xi^{\downarrow}(\mathbf{k})v^{n*}_{\mathbf{k}\downarrow} + \Delta^{\uparrow\downarrow}(-\mathbf{k})u^{n*}_{-\mathbf{k}\uparrow} \tag{2.32}$$

$$u^{n*}_{-\mathbf{k}\uparrow}E_{-\mathbf{k}n} = \xi^{\uparrow}(\mathbf{k})u^{n*}_{-\mathbf{k}\uparrow} + \Delta^{\uparrow\downarrow *}(-\mathbf{k})v^{n*}_{\mathbf{k}\downarrow} \tag{2.33}$$

These two sets of BdG equations tell us a very important property of these equations. To see this clearly, let us write equations (2.26-2.29) in a matrix eigenvalue equation, $M(\mathbf{k})\Phi_{\mathbf{k}} = E_{\mathbf{k}}\Phi_{\mathbf{k}}$,

$$\begin{pmatrix} \xi^{\uparrow}(\mathbf{k}) & \Delta^{\uparrow\downarrow}(\mathbf{k}) & 0 & 0 \\ \Delta^{\uparrow\downarrow *}(\mathbf{k}) & -\xi^{\downarrow}(-\mathbf{k}) & 0 & 0 \\ 0 & 0 & \xi^{\downarrow}(\mathbf{k}) & \Delta^{\uparrow\downarrow}(-\mathbf{k}) \\ 0 & 0 & \Delta^{\uparrow\downarrow *}(-\mathbf{k}) & -\xi^{\uparrow}(-\mathbf{k}) \end{pmatrix} \begin{pmatrix} u_{\mathbf{k}\uparrow} \\ v_{-\mathbf{k}\downarrow} \\ u_{\mathbf{k}\downarrow} \\ v_{-\mathbf{k}\uparrow} \end{pmatrix} = E_{\mathbf{k}} \begin{pmatrix} u_{\mathbf{k}\uparrow} \\ v_{-\mathbf{k}\downarrow} \\ u_{\mathbf{k}\downarrow} \\ v_{-\mathbf{k}\uparrow} \end{pmatrix} \tag{2.34}$$

Notice if we substitute $k \rightarrow \ -k$ in the second set of equations (2.30-2.33), take the complex conjugate and then compare it to the first set, we get,

$$\begin{pmatrix} \xi^{\uparrow}(-\mathbf{k}) & \Delta^{\uparrow\downarrow}(-\mathbf{k}) & 0 & 0 \\ \Delta^{\uparrow\downarrow *}(-\mathbf{k}) & -\xi^{\downarrow}(\mathbf{k}) & 0 & 0 \\ 0 & 0 & \xi^{\downarrow}(-\mathbf{k}) & \Delta^{\uparrow\downarrow}(\mathbf{k}) \\ 0 & 0 & \Delta^{\uparrow\downarrow *}(\mathbf{k}) & -\xi^{\uparrow}(\mathbf{k}) \end{pmatrix} \begin{pmatrix} -v^{*}_{-\mathbf{k}\uparrow} \\ u^{*}_{\mathbf{k}\downarrow} \\ v^{*}_{-\mathbf{k}\downarrow} \\ -u^{*}_{\mathbf{k}\uparrow} \end{pmatrix} = -E_{\mathbf{k}} \begin{pmatrix} -v^{*}_{-\mathbf{k}\uparrow} \\ u^{*}_{\mathbf{k}\downarrow} \\ v^{*}_{-\mathbf{k}\downarrow} \\ -u^{*}_{\mathbf{k}\uparrow} \end{pmatrix} \tag{2.35}$$

In the matrix form this would mean, $M(-\mathbf{k})\tilde{\Phi}_{\mathbf{k}} = -E_{\mathbf{k}}\tilde{\Phi}_{\mathbf{k}}$ where we define $\tilde{\Phi}_{\mathbf{k}} = K(\sigma_x \otimes \sigma_x)\Phi_{\mathbf{k}}$ and K is complex conjugate operator. This suggests that eigen-spectrum for $M(-\mathbf{k})$ can be known from just the eigen-spectrum of $M(\mathbf{k})$! By defining the transformation $\Theta \equiv K(\sigma_x \otimes \sigma_x)$, we can check this from either sets of BdG equations that,

$$\Theta M(\mathbf{k})\Theta^{-1} = -M(-\mathbf{k}) \tag{2.36}$$

This symmetry looks like the particle-hole symmetry since the negative energies of $M(-\mathbf{k})$ equals the positive energies of the $M(\mathbf{k})$, in fact this is actually the particle-

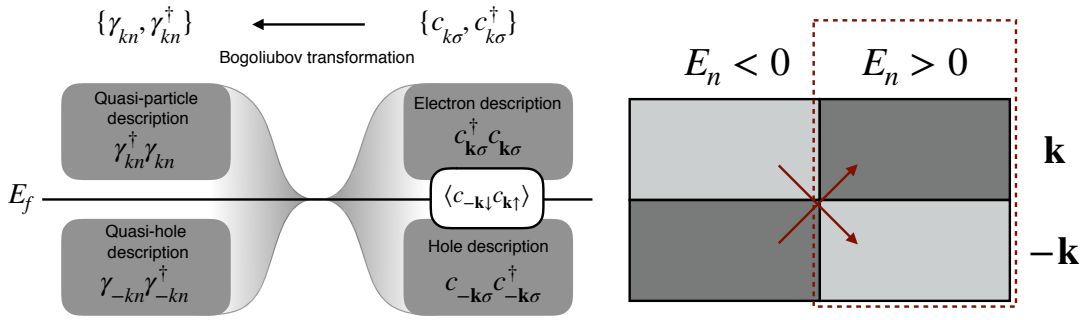

Figure 2.1.2: Pictorial representation of Bogoliubov-de Gennes method to solve a superconducting system.

hole symmetry of the Bogoliubov *quasi-particles* and Bogoliubov *quasi-holes*! It is evident since one set of BdG equations (for quasi-particles) came from comparing quasi-particle annihilation operators $\gamma_{\mathbf{k}}$ and the other set of equations (for quasi-holes) came from comparing $\gamma^\dagger_{-\mathbf{k}}$, which is just an *annihilation operator for quasi-hole* if we again do a quasiparticle-quasihole transformation to these operators. Also notice that since the Hamiltonian is diagonal in the Bogoliubov quasiparticle basis, we should choose to work with either quasi-particle (positive energy spectrum) or quasi-hole (negative energy spectrum) which is why we put a prime ($'$) as a constraint on the sum while defining the Bogoliubov transformations (2.23). Figure 2.1.2 shows how due to the presence of superconducting pairing terms we need to work in the redundant space of simultaneous descriptions of particle and hole. Finally, once the system is transformed into a new basis with Bogoliubov particles, we either choose to work with Bogoliubov particle or Bogoliubov holes to calculate the averages.

As a convention, we choose to work with positive energies and discard the negative energy contribution. It is clear that for each value of $\mathbf{k}$, we will obtain 4 energy eigenvalues and eigenvectors, in total we are going to end up with $4N_s$ eigenvalues and eigenvectors despite having only $2N_s$ degrees of freedom in our model (N_s lattice sites and 2 spins at each site). By choosing to work with either quasiparticle or quasiholes, we get rid of this redundancy and retain, in total, $2N_s$ degrees of freedom due to the particle-hole symmetric nature of our formalism. It is worthwhile to note that even though this property of the formalism is frequently termed as 'particle-hole symmetry', it is really a symmetry due to the *redundant description* and *not* a property of the underlying physics! It is also important to mention here that this 'particle-hole' symmetry will not be broken even if we include equal spin pairing (ESP) terms, that captures the

physics of triplet superconductivity, and spin-orbit coupling, therefore this approach is as general as it can be.

We have obtained a set of Bogoliubov-de Gennes equations using which we solve for the quasi-particle (and quasi-hole) spectrum. Using the spectrum of quasi-particles (positive energy solutions), we calculate the self-consistent averages, $\{\Delta_{SC}, \langle n_{\uparrow\downarrow}\rangle\}$ from their respective definitions by plugging in the transformation (2.23),

$$\begin{aligned}\Delta_\delta^\pm &= {\sum_n}' \left(e^{ik_\delta} u^n_{\mathbf{k}\uparrow} v^{n^*}_{-\mathbf{k}\downarrow} f(E_{\mathbf{k}n}) - e^{ik_\delta} u^n_{-\mathbf{k}\downarrow} v^{n^*}_{\mathbf{k}\uparrow} f(-E_{-\mathbf{k}n})\right) \\ &= {\sum_n}' \left(e^{ik_\delta} u^n_{\mathbf{k}\uparrow} v^{n^*}_{-\mathbf{k}\downarrow} f(E_{\mathbf{k}n}) - e^{-ik_\delta} u^n_{\mathbf{k}\downarrow} v^{n^*}_{-\mathbf{k}\uparrow} f(-E_{\mathbf{k}n})\right) \end{aligned} \tag{2.37}$$

where in the second step we replace $\mathbf{k}$ to $-\mathbf{k}$ since there is an overall summation. Notice that we had to make this replacement because from the eigen spectrum of $H(\mathbf{k})$ we can not obtain the $u_{-\mathbf{k}\downarrow}$ and $v_{\mathbf{k}\uparrow}$ elements of any eigenvector. Also, the prime on the summation is over n to include only positive energy eigen-spectrum. Similarly,

$$\langle n_\uparrow\rangle = {\sum_{\mathbf{k},n}}' \left(|u^n_{\mathbf{k}\uparrow}|^2 f(E_{\mathbf{k}n}) + |v^n_{-\mathbf{k}\uparrow}|^2 f(-E_{\mathbf{k}n})\right) \tag{2.38}$$

$$\langle n_\downarrow\rangle = {\sum_{\mathbf{k},n}}' \left(|u^n_{\mathbf{k}\downarrow}|^2 f(E_{\mathbf{k}n}) + |v^n_{-\mathbf{k}\downarrow}|^2 f(-E_{\mathbf{k}n})\right) \tag{2.39}$$

We can use these equations in general when but since our matrix $M(\mathbf{k})$ is block diagonalize, we make use of the symmetry property mentioned above and further simply these averages by mapping the negative energy solutions from $-\mathbf{k}$ sector to positive energy solutions of $\mathbf{k}$ sector as shown in figure 2.1.2,

$$\Delta_\delta^\pm = \sum_{\mathbf{k},n} e^{ik_\delta}\ u^n_{\mathbf{k}\uparrow} v^{n^*}_{-\mathbf{k}\downarrow} f(E_n) \tag{2.40}$$

$$\langle n_\uparrow\rangle = \sum_{\mathbf{k},n} |u^n_{\mathbf{k}\uparrow}|^2 f(E_{\mathbf{k}n}) \tag{2.41}$$

$$\langle n_\downarrow\rangle = \sum_{\mathbf{k},n} |v^n_{-\mathbf{k}\downarrow}|^2 f(-E_{\mathbf{k}n}) \tag{2.42}$$

Notice that the prime from the summation over n is now lifted since we map the negative

energy spectrum to the positive energy spectrum and work with only one of the 2×2 blocks of $M(\mathbf{k})$. Using these definitions, we define our SC order parameters (OP) defined in (2.10-2.13). These definitions have their usual meaning of $s$wave, $d$wave, $p$wave as introduced in chapter 1 and this can also be verified by the k-dependence of the corresponding gap function $\Delta^{\uparrow\downarrow}(\mathbf{k})$. As a side remark, if we had included $\uparrow\uparrow$ pairing and $\downarrow\downarrow$ pairing SC terms, the resulting 4×4 matrix would not have been block diagonal. These *like-like* spin pairing terms enter the off-diagonal block of the matrix[5]. That is when we use the definitions with restricted sum and hence is a consequence of the fact that we necessarily have to work in a redundant space in order to deal with superconductivity.

2.1.3 Real space formalism

The advantage of momentum space formalism is that by performing Fourier transform, we block diagonalize the full Hamiltonian and label each block by a quantum number k which is called the *crystal momentum*. The assumption that goes into having k as a *good* quantum number is that the system should be translationally invariant. In the presence of disorder (Nanguneri et al., 2012; Dobrosavljevic et al., 2012), or open boundaries, this property is lost and we are forced to work in real space where the equations will become cumbersome and thus require greater computational power. In this section, we will be carrying out similar analysis in real space as we did in the momentum space picture. Let us begin with the mean-field Hamiltonian (2.5) and generalize it to include disorder as,

$$\begin{aligned} H_{\text{eff}} = &\sum_{ij,\sigma} h_{ij\sigma} c^{\dagger}_{i\sigma} c_{j\sigma} - U \sum_{i} \left[\Delta_{ii} c^{\dagger}_{i\uparrow} c^{\dagger}_{i\downarrow} + \Delta^{*}_{ii} c_{i\downarrow} c_{i\uparrow} \right] \\ &- V \sum_{\langle i,j \rangle} \left[\Delta_{ij} c^{\dagger}_{i\uparrow} c^{\dagger}_{j\downarrow} - \Delta_{ji} c^{\dagger}_{i\downarrow} c^{\dagger}_{j\uparrow} + h.c. \right] + E_{\text{const}} \end{aligned} \tag{2.43}$$

where we have defined,

$$h_{ij\sigma} = -t_{ij\sigma} + (\epsilon_{i\sigma} - \mu_{\sigma})\delta_{ij} \tag{2.44}$$

$$\Delta_{ij} = \langle c_{j\downarrow} c_{i\uparrow} \rangle \tag{2.45}$$

[5]This also happens if we include spin-orbit coupling.

Notice that these potentials are now site and spin dependent. Randomly assigned values to these potentials model a spin-dependent disordered system. We introduce two additional parameters that quantify the amount of disorder in the system - hopping disorder V_t and on-site disorder V_e. These two parameters define the hopping parameters $t_{ij\sigma}$ and on-site potential $\epsilon_{i\sigma}$ as $t_{ij\sigma} = t_0 + \epsilon_t$ where ϵ_t is chosen randomly from a uniform distribution $P(\epsilon_t) = [-V_t, V_t]$ (Kumar et al., 2015). Similarly, $\epsilon_{i\sigma} = \epsilon_e$ where ϵ_t is chosen randomly from a uniform distribution $P(\epsilon_e) = [-V_e, V_e]$. By the introduction of the disorder, the translation symmetry will be broken. We now calculate the commutation relations with the electronic operators but now expressed in real space,

$$[c_{i\uparrow}, \mathcal{H}_{\text{eff}}] = \sum_j h_{ij\uparrow} c_{j\uparrow} - \sum_j \Delta_{ij}^{\uparrow\downarrow} c_{j\downarrow}^\dagger \tag{2.46}$$

$$[c_{i\uparrow}^\dagger, \mathcal{H}_{\text{eff}}] = -\sum_j h_{ij\uparrow} c_{j\uparrow}^\dagger + \sum_j \Delta_{ij}^{\uparrow\downarrow *} c_{j\downarrow} \tag{2.47}$$

$$[c_{i\downarrow}, \mathcal{H}_{\text{eff}}] = \sum_j h_{ij\downarrow} c_{j\downarrow} + \sum_j \Delta_{ji}^{\uparrow\downarrow} c_{j\uparrow}^\dagger \tag{2.48}$$

$$[c_{i\downarrow}^\dagger, \mathcal{H}_{\text{eff}}] = -\sum_j h_{ij\downarrow} c_{j\downarrow} - \sum_j \Delta_{ji}^{\uparrow\downarrow *} c_{j\uparrow}^\dagger \tag{2.49}$$

Since these commutation relations mix up particle sector and hole sector, we define a transformation,

$$c_{i\sigma} = \sum_n{}' \left(u_{i\sigma}^n \gamma_n - \sigma v_{i\sigma}^{n^*} \gamma_n^\dagger \right) \longleftrightarrow c_{i\sigma}^\dagger = \sum_n{}' \left(u_{i\sigma}^{n^*} \gamma_n^\dagger - \sigma v_{i\sigma}^n \gamma_n \right) \tag{2.50}$$

using this transformation, we again diagonalize the effective Hamiltonian in the same form as in equation (2.25) and obtain $4N_s$ coupled BdG equations,

$$E_n u_{i\uparrow}^n = \sum_j h_{ij\uparrow} u_{j\uparrow}^n - \sum_j \Delta_{ij} v_{j\downarrow}^n \tag{2.51}$$

$$E_n u_{i\downarrow}^n = \sum_j h_{ij\downarrow} u_{j\downarrow}^n - \sum_j \Delta_{ji} v_{j\uparrow}^n \tag{2.52}$$

$$E_n v_{i\uparrow}^n = -\sum_j h_{ij\uparrow} v_{j\uparrow}^n - \sum_j \Delta_{ij}^* u_{j\downarrow}^n \tag{2.53}$$

$$E_n v_{i\downarrow}^n = -\sum_j h_{ij\downarrow} v_{j\downarrow}^n - \sum_j \Delta_{ji}^* u_{j\uparrow}^n \tag{2.54}$$

This set of BdG equations can be cast into a matrix form:

$$\sum_j M_{ij}\phi_j = E_n\phi_i \tag{2.55}$$

Here, ϕ_i is a four-component vector and M_{ij} is correspondingly $4x4$ matrix as,

$$\phi_i \equiv \begin{pmatrix} u^n_{i\uparrow} \\ v^n_{i\downarrow} \\ u^n_{i\downarrow} \\ v^n_{i\uparrow} \end{pmatrix} \qquad M_{ij} \equiv \begin{pmatrix} h_{ij\uparrow} & \Delta_{ij} & 0 & 0 \\ \Delta^*_{ji} & -h_{ij\downarrow} & 0 & 0 \\ 0 & 0 & h_{ij\downarrow} & \Delta_{ji} \\ 0 & 0 & \Delta^*_{ij} & -h_{ij\uparrow} \end{pmatrix} \tag{2.56}$$

Notice M_{ij} is just a block of the full $4N_s \times 4Ns$ matrix where i, j are site indices and run from 1 to N_s each. This again means we will obtain a total of $4N_s$ eigenvalues and eigenvectors which is more than the number of degrees of freedom we have in our model. To get rid of this, we make use of the symmetry we introduced earlier but now expressed in the real space basis as,

$$\begin{pmatrix} u^n_{i\uparrow} \\ v^n_{i\downarrow} \\ u^n_{i\downarrow} \\ v^n_{i\uparrow} \end{pmatrix} \rightarrow \begin{pmatrix} -v^{\bar{n}*}_{i\uparrow} \\ u^{\bar{n}*}_{i\downarrow} \\ v^{\bar{n}*}_{i\downarrow} \\ -u^{\bar{n}*}_{i\uparrow} \end{pmatrix} = K(\sigma^i_y \otimes \sigma^i_y) \begin{pmatrix} u^n_{i\uparrow} \\ v^n_{i\downarrow} \\ u^n_{i\downarrow} \\ v^n_{i\uparrow} \end{pmatrix} \tag{2.57}$$

We would like to mention this again that the Bogoliubov transformation considered earlier is a most general transformation one can write. That means the sum over n does not guarantee that when this transformation is used to diagonalize the Hamiltonian $H = \sum_n E_n\gamma^\dagger_n\gamma_n + E_{\text{const}}$, we get positive excitation spectrum. We therefore ask for only those n which correspond to a positive excitation energy, i.e. positive eigenvalues $E_n \geq 0$. Which is why we put a constraint (marked by $'$ on the sum) on the summation of equation (2.50) indicating only those n are considered which later gives positive exception spectrum. You can notice that this symmetry will hold irrespective of the presence/absence of time reversals symmetry therefore, if one latter includes Zeeman field terms in the chemical potential, this should still hold! It is ironic that the redundancy actually entered through the Bogoliubov transformation (2.50) itself since there is no way of removing the terms before diagonalising we went ahead and arrived at the BdG relations and then remove those solutions which correspond to negative en-

ergy. This is as general as it can be except for the fact we are not considering case where *like-like* pairing and spin-orbit coupling is present. In the presence of *like-like* SC pairing and spin-orbit terms we can still show that redundancy is present using the same mapping as (2.57).

In the definition of $\Delta_{ij} = \langle c_{j\downarrow} c_{i\uparrow} \rangle$, substituting the transformation for the electronic operators and using the fact that at non-zero temperature $\langle \gamma_n^\dagger \gamma_m \rangle = f(E_n)\delta_{nm}$, where f is the Fermi-Dirac function, we obtain the self consistent definition of the averages,

$$\Delta_{ij} = \sum_n{}' \left(u_{i\uparrow}^n v_{j\downarrow}^{n^*} f(E_n) - u_{j\downarrow}^n v_{i\uparrow}^{n^*} f(-E_n) \right) \tag{2.58}$$

$$\langle n_{i\uparrow} \rangle = \sum_n{}' \left(|u_{i\uparrow}^n|^2 f(E_n) + |v_{i\uparrow}^n|^2 f(-E_n) \right) \tag{2.59}$$

$$\langle n_{i\downarrow} \rangle = \sum_n{}' \left(|v_{i\downarrow}^n|^2 f(-E_n) + |u_{i\downarrow}^n|^2 f(E_n) \right) \tag{2.60}$$

Again, by making use of the symmetry transformation (2.57), we simplify these equations to,

$$\Delta_{ij} = \sum_n u_{i\uparrow}^n v_{j\downarrow}^{n^*} f(E_n) \tag{2.61}$$

$$\langle n_{i\uparrow} \rangle = \sum_n |u_{i\uparrow}^n|^2 f(E_n) \tag{2.62}$$

$$\langle n_{i\downarrow} \rangle = \sum_n |v_{i\downarrow}^n|^2 f(-E_n) \tag{2.63}$$

where the sum is now unrestricted and we work with only upper block of the matrix equation (2.56). Using these relations, we calculated the averages to characterize the SC order. In the next section we explore how do we implement the self consistent approach computationally.

2.1.4 A comment on implementation of self-consistent method

Before we proceed to results, it is important to understand how the method of self-consistency is implemented computationally. We set electronic hopping $t = 1$ as the basic energy scale, then we are left with four independent parameters in the Hamilto-

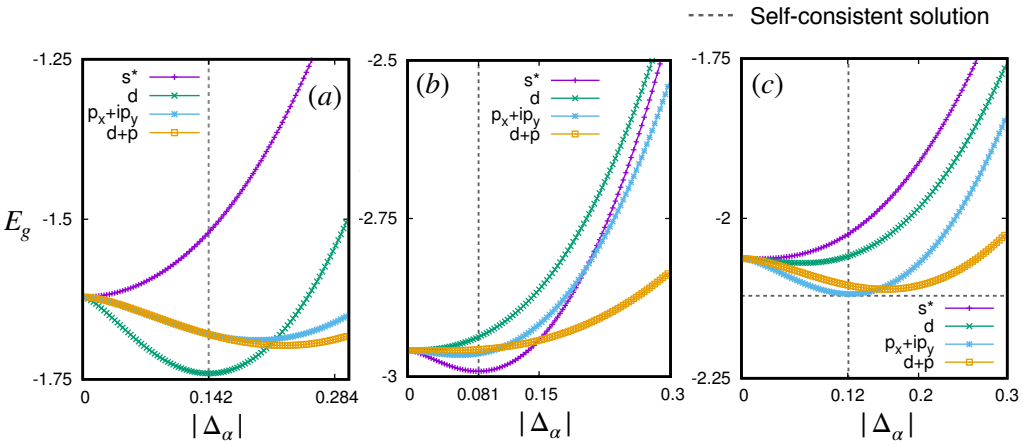

Figure 2.1.3: Ground state energy variation w.r.t. the magnitude of various SC OP. The minima lies where the self-consistent solution converges.

nian, *viz.*, U, V, T, and μ. Corresponding to these, we will obtain a set of self-consistent SC pairing correlations, $\{\Delta\}$ that defines the SC OP using the relation (2.10-2.13). To solve the BdG equations numerically, an initial guess of $\{\Delta\}$ and $\{\langle n_\sigma \rangle\}$ is fed into the Hamiltonian. This Hamiltonian is diagonalized and eigenvalues and eigenvectors are calculated. The obtained eigenspectrum is used to further redefine the Hamiltonian and is rediagonalized. This set of steps is labelled as an iteration and the cycle of iteration is repeated until the averages converge within a specified error, which was set to 10^{-5} in our calculations. The ground state (at $T = 0$) energy is calculated by summing over all the negative energy states and E_{const} which is given by the expression (2.18). Therefore, the problem now reduces to minimizing the total energy w.r.t. the set $\{\Delta\}$ of pairing correlations. Since we do not fix any constraint on the nature of the pairing correlation, energy minimization shall result is the most energetically favourable pairing correlation symmetries that may either by singlet like or triplet like or even some strange combination of these two! This method of calculating averages self-consistently is actually equivalent to the energy minimization. This can be seen from figure (2.1.3) which corresponds to three different starting configurations $\{U, V, T, \mu\}$ and shows how the solution obtained from self-consistent approach is equivalent to energy minimization.

You might also have noticed that in self-consistent calculations, we have no control over the final converged particle density. By changing the initial parameter configuration $\{U, V, T, \mu\}$, self-consistent calculation may lead to different particle density! We therefore need to have some control over this as it will become pointless to com-

pare phases with different density. We achieve this by changing the chemical potential within the code so that the converged density is close to (within some error) the desired density.

2.2 Bilayer model for proximity effect

We have seen how a superconductor can be modelled using BdG approach. We now construct a hypothetical model of a 2 dimensional superconducting layer in contact with a 2 dimensional metallic layer. The 'contact' can be via *inter-layer* hopping, neighbouring interactions, etc. but we will limit our calculations only to inter-layer hopping. The motivation behind this model is to explore proximity effect of a superconductor. A visual representation of this bilayer model is depicted in figure (2.2.1). We will later observe that interlayer hopping is enough to demonstrate proximity effect. We model a metallic system just by having *intra-layer* hopping terms and a chemical potential for layer 2. To avoid complexity, we will stick to the momentum space representation hence we assume translational invariance that comes from periodic boundaries and site independent potentials. The full model Hamiltonian is given by,

$$\begin{aligned}
H &= H_1 + H_2 + H_{12}, \\
H_1 &= -t_1 \sum_{\langle ij\rangle,\sigma} [c^\dagger_{i\sigma 1} c_{j\sigma 1} + H.c.] - \mu_1 \sum_{i\sigma} c^\dagger_{i\sigma 1} c_{i\sigma 1} \\
&\quad - U \sum_i n_{i\uparrow 1} n_{i\downarrow 1} - V \sum_{\langle ij\rangle} n_{i1} n_{j1}, \\
H_2 &= -t_2 \sum_{\langle ij\rangle,\sigma} [c^\dagger_{i\sigma 2} c_{j\sigma 2} + H.c.] - \mu_2 \sum_{i\sigma} c^\dagger_{i\sigma 2} c_{i\sigma 2}, \\
H_{12} &= -\tilde{t} \sum_{i\sigma} [c^\dagger_{i\sigma 1} c_{i\sigma 2} + H.c.].
\end{aligned} \tag{2.64}$$

Here again, $c_{i\sigma l}(c^\dagger_{i\sigma l})$ annihilates (creates) an electron in layer l at site i with spin σ, $\langle ij\rangle$ implies that sites i and j are nearest neighbours within a layer. μ_l is the layer-dependent chemical potential, with $\Delta\mu \equiv \mu_1 - \mu_2$ being equivalent to gate potential. The layer-resolved local number operators are given by $n_{i\sigma l} = c^\dagger_{i\sigma l} c_{i\sigma l}$, and $n_{il} = n_{i\uparrow l} + n_{i\downarrow l}$. Notice that the interaction terms (U and V) are only defined on layer 1 ($l = 1$) which will behave as a superconductor in the limit $\tilde{t} \to 0$. In this limit the H_1 and H_2 decouple from each other and we recover our monolayer model, we explored in the previous sec-

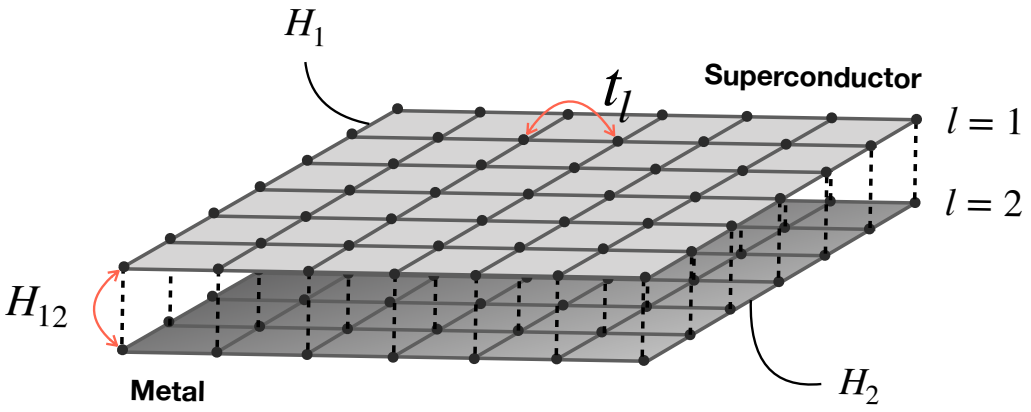

Figure 2.2.1: Visual representation of the bilayer model: 2D SC layer in proximity to a metallic layer.

tion, along with a tight-binding model that represents a metal. When there is coupling between these two layers $H_{12} \neq 0$, the system behave as one and interesting physics can be explored. We will set $t_1 = 1$ as the basic energy scale, and restrict ourselves to zero temperatures ($T = 0$), then we are left with six independent parameters in the Hamiltonian, *viz.*, t_2, $\tilde{t}$, U, V, μ_1 and μ_2. We now apply the Bogoliubov-de Gennes mean-field approach to this model and arrive at a single particle mean field Hamiltonian,

$$H = \sum_{\mathbf{k}} \Bigg(\sum_{\sigma,l} \xi_l(\mathbf{k}) c^\dagger_{\mathbf{k}\sigma l} c_{\mathbf{k}\sigma l} + \left[\Delta_1^{\uparrow\downarrow}(\mathbf{k}) c^\dagger_{\mathbf{k}\uparrow 1} c^\dagger_{-\mathbf{k}\downarrow 1} + H.c. \right] - \tilde{t} \sum_{\sigma} \left[c^\dagger_{\mathbf{k}\sigma 1} c_{\mathbf{k}\sigma 2} + c^\dagger_{\mathbf{k}\sigma 2} c_{\mathbf{k}\sigma 1} \right] \Bigg) \tag{2.65}$$

where,

$$\xi_l(\mathbf{k}) = -2t_l(\cos k_x + \cos k_y) - \mu_l \tag{2.66}$$

$$\Delta^{\uparrow\downarrow}(\mathbf{k}) = -U\Delta_0 - V(e^{-ik_x}\Delta_x^+ + e^{ik_x}\Delta_x^- + e^{-ik_y}\Delta_y^+ + e^{ik_y}\Delta_y^-) \tag{2.67}$$

The commutation relations of the mean-field Hamiltonian with the electronic creation and annihilation operators are given by,

$$\left[c_{\mathbf{k}\uparrow 1}, H^{MF}\right] = \xi_1(\mathbf{k}) c_{\mathbf{k}\uparrow 1} + \Delta^{\uparrow\downarrow}(\mathbf{k}) c^{\dagger}_{-\mathbf{k}\downarrow 1} - \tilde{t} c_{\mathbf{k}\uparrow 2}, \tag{2.68}$$

$$\left[c^{\dagger}_{-\mathbf{k}\downarrow 1}, H^{MF}\right] = -\xi_1(-\mathbf{k}) c_{-\mathbf{k}\downarrow 1} + \Delta^{\uparrow\downarrow *}(\mathbf{k}) c^{\dagger}_{\mathbf{k}\uparrow 1} + \tilde{t} c_{-\mathbf{k}\downarrow 2}, \tag{2.69}$$

$$\left[c_{\mathbf{k}\uparrow 2}, H^{MF}\right] = \xi_2(\mathbf{k}) c_{\mathbf{k}\uparrow 2} - \tilde{t} c_{\mathbf{k}\uparrow 1}, \tag{2.70}$$

$$\left[c^{\dagger}_{-\mathbf{k}\downarrow 2}, H^{MF}\right] = -\xi_2(-\mathbf{k}) c_{-\mathbf{k}\downarrow 2} + \tilde{t} c_{-\mathbf{k}\downarrow 1}. \tag{2.71}$$

Note that instead of writing the commutation relations using $\{c_{\mathbf{k}\uparrow l}, c_{\mathbf{k}\downarrow l}\}$ we write them it terms of $\{c_{\mathbf{k}\uparrow l}, c^{\dagger}_{-\mathbf{k}\downarrow l}\}$ which is also an independent set. From these equations we see that since we are already working in momentum-space, the Hamiltonian was already block diagonalized. Therefore, we did not get a sum over all creation (annihilation) operators like we did in real space. We now use a similar Bogoliubov transformation, motivated by the fact that it should mix creation and annihilation electronic operators.

$$c_{\mathbf{k}\sigma l} = \sum_{n}{}' \left(u^{n}_{\mathbf{k}\sigma l}\gamma_n - \sigma v^{n^*}_{\mathbf{k}\sigma l}\gamma^{\dagger}_n\right) \longleftrightarrow c^{\dagger}_{\mathbf{k}\sigma l} = \sum_{n}{}' \left(u^{n^*}_{\mathbf{k}\sigma l}\gamma^{\dagger}_n - \sigma v^{n}_{\mathbf{k}\sigma l}\gamma_n\right) \tag{2.72}$$

On plugging this transformation in the above commutation relations diagonalize the Hamiltonian to give us 8 (expanding $l = 1, 2$) BdG equations out of which only 4 are independent (as stated earlier):

$$u^{n}_{\mathbf{k}\uparrow 1} E_n = \xi_1(\mathbf{k}) u^{n}_{\mathbf{k}\uparrow 1} + \Delta^{\uparrow\downarrow}(\mathbf{k}) v^{n}_{-\mathbf{k}\downarrow 1} - \tilde{t} u^{n}_{\mathbf{k}\uparrow 2} \tag{2.73}$$

$$v^{n}_{-\mathbf{k}\downarrow 1} E_n = -\xi_1(-\mathbf{k}) v^{n}_{-\mathbf{k}\downarrow 1} + \Delta^{\uparrow\downarrow *}(\mathbf{k}) u^{n}_{\mathbf{k}\uparrow 1} + \tilde{t} v^{n}_{-\mathbf{k}\downarrow 2} \tag{2.74}$$

$$u^{n}_{\mathbf{k}\uparrow 2} E_n = \xi_2(\mathbf{k}) u^{n}_{\mathbf{k}\uparrow 2} - \tilde{t} u^{n}_{\mathbf{k}\uparrow 1} \tag{2.75}$$

$$v^{n}_{-\mathbf{k}\downarrow 2} E_n = -\xi_2(-\mathbf{k}) v^{n}_{-\mathbf{k}\downarrow 2} + \tilde{t} v^{n}_{-\mathbf{k}\downarrow 1} \tag{2.76}$$

These equations can be cast into a 4×4 matrix form for each k. Bilayer model follows from direct generalization of a single layer model discussed in the previous sections. Therefore, instead of a $2N \times 2N$ matrix, we will have to solve a $4N \times 4N$ matrix that follows from the fact that we have now increased the number of degrees of freedom.

$M(\mathbf{k})\Phi(\mathbf{k}) = E\Phi(\mathbf{k})$ where the matrices look like,

$$\Phi(\mathbf{k}) \equiv \begin{pmatrix} u^n_{\mathbf{k}\uparrow 1} \\ v^n_{-\mathbf{k}\downarrow 1} \\ u^n_{\mathbf{k}\uparrow 2} \\ v^n_{-\mathbf{k}\downarrow 2} \end{pmatrix} \; M(\mathbf{k}) \equiv \begin{pmatrix} \xi_1(\mathbf{k}) & \Delta^{\uparrow\downarrow}(\mathbf{k}) & -\tilde{t} & 0 \\ \Delta^{\uparrow\downarrow *}(\mathbf{k}) & -\xi_1(-\mathbf{k}) & 0 & \tilde{t} \\ -\tilde{t} & 0 & \xi_2(\mathbf{k}) & 0 \\ 0 & \tilde{t} & 0 & -\xi_2(-\mathbf{k}) \end{pmatrix} \tag{2.77}$$

These equations defined for each $\mathbf{k}$ will result in 4 eigen-solutions; solving N_s such equations defined on the Brillouin zone will give us a total of 4 N_s eigen-solutions that are used to self-consistently define the averages: $\{\Delta\}$ and $\langle N\rangle$.

$$\Delta_{o,l} = \frac{1}{N_s}\sum_{\mathbf{k}n} u^n_{\mathbf{k}\uparrow l} v^{n*}_{-\mathbf{k}\downarrow l} f(E_n) \tag{2.78}$$

$$\Delta^{\pm}_{x,l} = \frac{1}{N_s}\sum_{\mathbf{k}n} e^{\pm ik_x}\; u^n_{\mathbf{k}\uparrow l} v^{n*}_{-\mathbf{k}\downarrow l} f(E_n) \tag{2.79}$$

$$\Delta^{\pm}_{y,l} = \frac{1}{N_s}\sum_{\mathbf{k}n} e^{\pm ik_y}\; u^n_{\mathbf{k}\uparrow l} v^{n*}_{-\mathbf{k}\downarrow l} f(E_n) \tag{2.80}$$

$$\langle N_{\uparrow l}\rangle = \frac{1}{N_s}\sum_{\mathbf{k}n} |u^n_{\mathbf{k}\uparrow l}|^2 f(E_n) \tag{2.81}$$

$$\langle N_{\downarrow l}\rangle = \frac{1}{N_s}\sum_{\mathbf{k}n} |v^n_{-\mathbf{k}\downarrow l}|^2 f(-E_n) \tag{2.82}$$

Where $f(\cdot)$ is the usual Fermi function that is introduced as $\langle \gamma^\dagger_n \gamma_n\rangle = f(E_n)$. It is important to mention here that the tight binding model, from which the BdG equations are derived, originates from the $t-J$ or the superexchange model which is a strongly correlated system (Kotliar et al., 1988). Nevertheless, it is fascinating how solutions of repulsive Hubbard model and attractive Hubbard model are very much alike.

2.3 Topological insulators and superconductors

Topological insulators, a recent development in condensed matter physics, has attracted attention of many scientists (Moore, 2010). These are electronic materials that have a bulk band gap like an ordinary insulator but have *protected* conducting states on their edge or surface (Hasan et al., 2010). In this section, we will first briefly introduce some

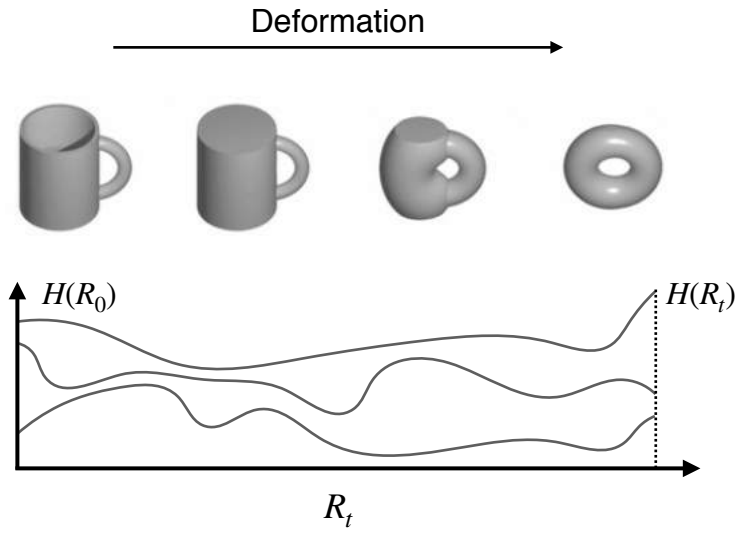

Figure 2.3.1: Topological equivalence of two manifolds and two Hamiltonians. Notice how the bands do not cross i.e., the 'topology of bands' relative to each other do not change.

concepts of topological band theory[6] and then apply these concepts to the superconducting model we introduced in the previous section.

Just as we understand topological equivalence for manifolds - deforming a coffee mug into a doughnut - one can imagine *tuning the Hamiltonian*, w.r.t. some parameter, so as to deform the band structure continuously between the two **without closing the energy gap**. Such a process defines a topological equivalence between different insulating states. Here the 'topology of the bands' is what we are interested in (Kruthoff et al., 2017) and whether if different Hamiltonians are connected by a smooth deformation tells us if they fall in the same topological equivalence class (Asbóth et al., 2016). This idea of classifying different insulating states based on their topological equivalence becomes necessary due to some non-trivial existence of states at the boundary (Shen, 2017). This is known as the *bulk-boundary correspondence*, which relates the topological structure of bulk crystal to the presence of *gap-less* boundary modes. This connection was first pointed out in quantized Hall conductance in quantum Hall effect as originating due to accumulation of Berry phase (Thouless et al., 1982). The common theme here between an insulators and superconductors is the gapped spectrum[7], which

[6]It is truly fascinating that topological insulators can be understood within the framework of the band theory of solids since the single-particle energy gap is not modified by electron-electron interactions in an essential way.

[7]Of course this is not valid for $d$wave superconductor which has a Dirac cone like band structure,

allows us to do a similar classifications of different gapped states and look for gap-less edge modes at the boundary (Qi et al., 2011). The classification of different 'vacuum states', is done via calculating their topological invariant - Chern number. Chern invariant is like 'genus' invariant of a manifold; the origin however is physical. An adiabatic transformation of Bloch wavefunctions around a closed loop results in accumulation of a geometric phase factor which may result in a non-zero Berry phase (Bernevig et al., 2013) given by the line integral $A_n(\mathbf{k}) = i\langle n(\mathbf{k})|\nabla_{\mathbf{k}}|n(\mathbf{k})\rangle$, for higher dimensions, it may be expressed as a surface integral of the Berry Curvature, $F_n(\mathbf{k}) = \nabla \times A_n(\mathbf{k})$. The Chern invariant is then defined as the total Berry flux in the Brillouin zone,

$$C_n = \frac{1}{2\pi}\int_{\text{BZ}} d^2\mathbf{k} F_n(\mathbf{k}) \tag{2.83}$$

One thing to note from here is that the Chern number, like the genus, is quantized[8], therefore, one cannot simply change the Chern number by small deformations. By the bulk-boundary correspondence, the Chern invariant relates to the existence of boundary states which we will soon see in the next chapter.

2.3.1 Chern numbers in Discrete BZ: Efficient method

We now need to use the discrete version of the formula to calculate Chern number since we work with discrete Brillouin zone while performing all calculations computationally. A straightforward approach for computing the Chern number would be to replace all the derivatives by discrete differences and the integral by a summation. The Berry connection, for instance, can be written as,

$$A_\mu(\mathbf{k})\delta\mathbf{k}_\mu = \langle n(\mathbf{k})|\delta_\mu|n(\mathbf{k})\rangle \tag{2.84}$$

where δ_μ is the difference operator $\delta_\mu f(\mathbf{k}) = f(\mathbf{k}+\delta\mathbf{k}_\mu) - f(\mathbf{k})$ and $\delta\mathbf{k}_\mu$ is the smallest displacement vector in the direction of μ. Note that while taking the differences of a state vector, we need to keep the local gauge with which the state $|n(\mathbf{k})\rangle$ is smoothly

hence is not gapped.

[8]It is because if one defined a unit vector $\hat{h}(\mathbf{k}) = h(\mathbf{k})/|h(\mathbf{k})|$, where $h(\mathbf{k})$ is defined using the single particle Hamiltonian as $H(\mathbf{k}) = h(\mathbf{k}) \cdot \vec{\sigma}$. Then Chern invariant simply counts the number of times $\hat{h}(\mathbf{k})$ wraps around the unit sphere as a function of $\mathbf{k}$.

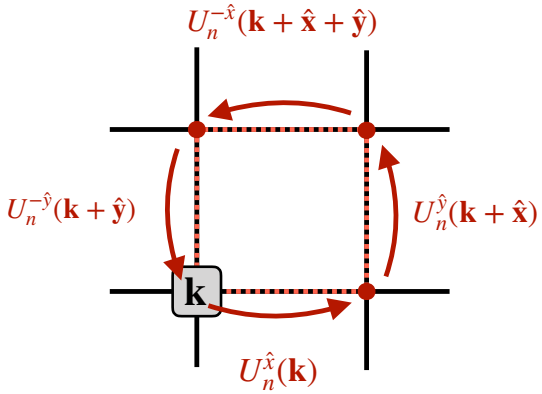

Figure 2.3.2: Pictorial representation of Berry phase calculation for discrete Brilluoin zone.

differentiable near $\mathbf{k}$. The Berry curvature is then defined as,

$$F_{\mu\nu}(\mathbf{k})\delta\mathbf{k}_\mu\delta\mathbf{k}_\nu = \left[\delta_\mu A_\nu(\mathbf{k}) - \delta_\nu A_\mu(\mathbf{k})\right]\delta\mathbf{k}_\mu\delta\mathbf{k}_\nu \tag{2.85}$$

Summing this quantity over the entire Brilluoin zone under a limit $\delta\mathbf{k}_\mu \to 0$, gives the chern number. Note that this direct procedure can become computationally heavy especially when the Hamiltonian is complicated. We therefore employ an efficient method to calculate Chern numbers, in the discrete Brillouin zone, introduced in the work (Fukui et al., 2005), by defining a $U(1)$ link variable, that encodes the phase information.

$$U_n^{\hat{\epsilon}}(\mathbf{k}) = \frac{\langle n(\mathbf{k})|n(\mathbf{k}+\hat{\epsilon})\rangle}{|\langle n(\mathbf{k})|n(\mathbf{k}+\hat{\epsilon})\rangle|} \tag{2.86}$$

Here, $\hat{\epsilon}$ is a vector in the $k_x - k_y$ plane that connects nearest neighbour points in the Brillouin zone. The index n denotes the band index. Note that since we're taking the inner product of two states, it is obvious that the phase will be gauge invariant. Summing this phase along a plaquette, in our case a square plaquette, gives us local Berry curvature,

$$F_n(\mathbf{k}) = \frac{1}{i}\ln\left[U_n^{\hat{\mathbf{x}}}(\mathbf{k})U_n^{\hat{\mathbf{y}}}(\mathbf{k}+\hat{\mathbf{x}})U_n^{-\hat{\mathbf{x}}}(\mathbf{k}+\hat{\mathbf{x}}+\hat{\mathbf{y}})U_n^{-\hat{\mathbf{y}}}(\mathbf{k}+\hat{\mathbf{y}})\right] \tag{2.87}$$

Note that the Berry curvature is defined within the principle branch of the logarithm, $-\pi < F_n(\mathbf{k}) \leq \pi$. Summing it over the Brillouin zone gives the Chern number for the

n^{th} band,

$$C_n = \frac{1}{2\pi} \sum_{\mathbf{k}} F_n(\mathbf{k}) \tag{2.88}$$

This alternate method is much more efficient than the direct calculation that involves calculation of derivatives of the eigenstates. First of all, this method is manifestly gauge invariant because of the use of inner products. Secondly, it is shown that this method strictly results in an integer therefore, even with a coarse discrete Brilluoin zone this shall work thereby making it efficient. The reader is advised to refer to (Fukui et al., 2005) which also provides a proof to why this method results in an integer.

Chapter 3

Results and Discussion

All the results produced during this work are presented in this chapter. For numerical diagonalization and reiterating the self-consistent method, Fortran 95 was used as the basic language along with GNU fortran compiler and LAPack package for linear algebra. All the plots and figures are made using gnuplot version 5.0.

3.1 Superconducting solution

We first plot the particle density of states (DOS) for a $d-$wave superconductor. Figure 3.1.2 plot (a) is just a familiar tight-binding density of states in two-dimensions. As the SC $d-$wave order Δ is turned on, a gap exactly at Fermi energy E_f starts opening up. The $d-$wave SC gap has a distinctive Dirac cone like structure unlike a clean $s-$wave gap. The density of states was plotted using the Lorentzian density function defined as $d(E) = \sum_{\text{states}} \frac{\gamma/\pi}{\gamma^2+(E-E_i)^2}$ with Lorenz broadening $\gamma = 0.01$. The fluctuations seen on the plot are due to the finite size of the lattice, here we used a lattice size $N_s = 300$.

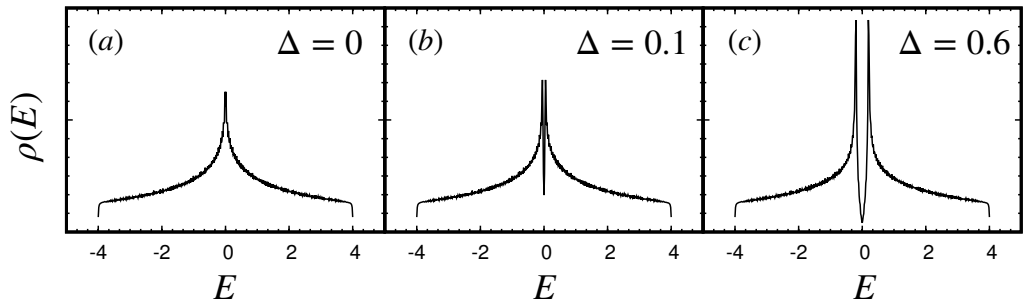

Figure 3.1.1: Particle density of states as $d-$wave SC order is introduced.

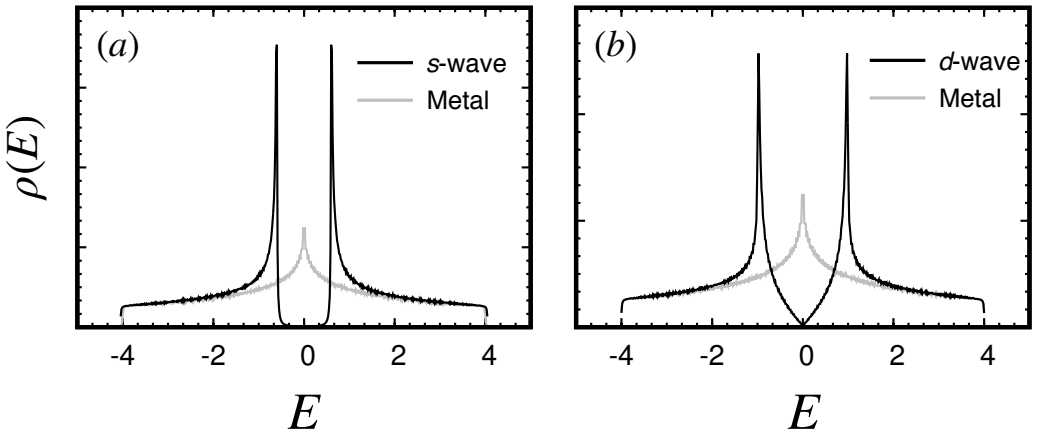

Figure 3.1.2: Quasi-particle DOS for (a) $s-$wave and (b) $d-$wave superconductor. Lorenz broadening used $\gamma = 0.01$.

We therefore confirm the existence of the $d-$wave superconducting order by looking at the density of states which clearly shows the $d-$wave gap and also the local SC gap function $\Delta^{\uparrow\downarrow}(\mathbf{k})$ which results in a similar plot as shown in figure 1.1.1 plot **A**. In figure 3.1.2 we show the particle density of states for the conventional $s-$ wave order and unconventional $d-$wave order. Notice how DOS only changes near the Fermi energy reflecting the fact that Cooper pairing takes place near the Fermi surface. This also reflects the fact that farther we go from the Fermi surface, the Bogoliubov quasiparticle attains more electron-like (or hole-like) character.

Next, we do a few checks to ensure the symmetry that we presented in equation (2.57). Recall, since we have a block diagonal matrix (2.56), we could map all the negative states from lower block to the positive states of the upper block and then consider the total spectrum of the upper block only to calculate averages. We concluded that one of the blocks in the Hamiltonian is enough to give the whole spectrum of eigenstates in the system - this statement is general, whether the system has disorder or not! If there is, additionally, spin degeneracy in the system, as in the case of spin-independent disorder, the spectrum generated with one of the blocks in the Hamiltonian will be symmetric about zero energy. Furthermore, this same spectrum can also be generated with the other block of the Hamiltonian. Now if we break the time reversal symmetry, the symmetric spectrum generated by the blocks is lost. In this case, even though we did prove the $E/-E$ symmetry due to redundancy, we would like to test this numerically. Figure 3.1.3-(a) shows the energy spectrum of the two blocks. The spectrum of the top

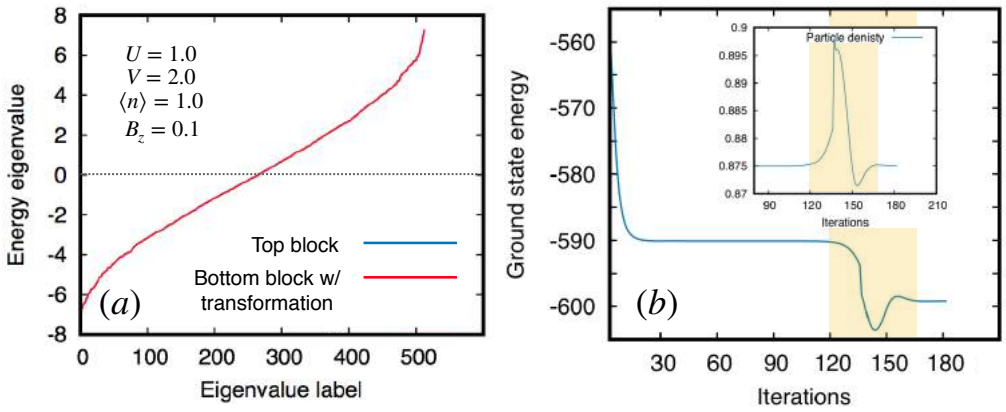

Figure 3.1.3: (a) Energy spectrum of two blocks from equation (2.56), (b) Ground state energy variation with iteration, inset: particle density variation with iteration.

block is plotted as it is, but the spectrum of the lower block is multiplied by -1 and then plotted to match it with the spectrum of the top block. We can see the two spectra exactly matches even when the time reversal symmetry is absent. This fact allows us to work with one of the blocks and discard the other without even worrying about the presence of time reversal symmetry. A real space matrix was chosen for analysing the spectrum, shown in figure 3.1.3, in the presence of spin-dependent disorder (on-site and hopping) with disorder strength $V_e = V_t = 2.0$ and Magnetic field strength $B_z = 0.1$. This matching was also performed when the initial Δs are randomly assigned (at each site) which also resulted in confirming the $E/-E$ symmetry. Therefore one can always choose to work with one of the blocks with appropriate mapping.

Next we monitor the ground state energy as self-consistency loop progresses and is shown in figure 3.1.3-(b). The self-consistency loop converges at around 180th iteration. Note that we had shown earlier that self consistency is equivalent to energy minimization. From figure 3.1.3-(b) it seems like the least energy solution is not preferred. The parameter choice is $U = 3.2, V = 2.0, \langle N \rangle = 0.875$ where the density is held fixed by changing the chemical potential dynamically as the self-consistency loop progresses. As can be seen, the energy decreases with iterations - there is however a point (around 150th iteration) where it has increased, this is due to the fact that in the code the particle density is maintained to a desired value, which is $\langle N \rangle = 0.875$. As the energy decreases the particle density increases, see inset yellow region, but we do not want that solution, the re-adjustment of chemical potential forces the ground state energy to increase which corresponds to a minima with constraint on particle density.

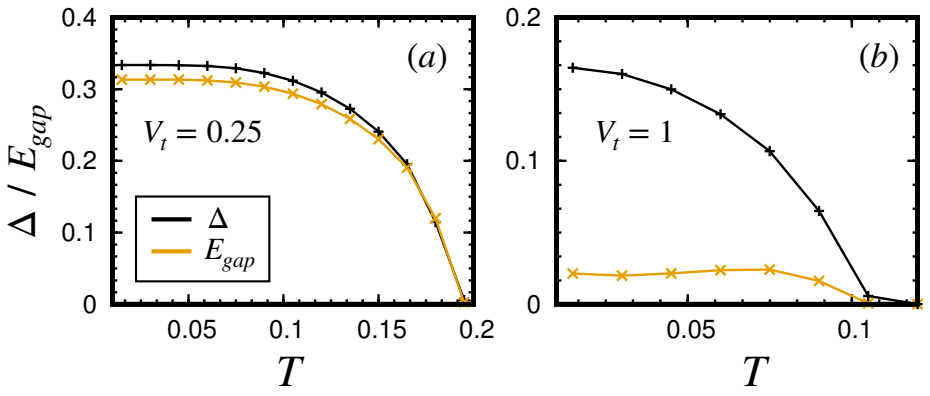

Figure 3.2.1: E_{gap} and Δ variation with temperature at different disorder strengths.

This was further verified when the density fixing was turned off and density was left to converge to any desired value: no ground state energy rise was observed with iteration. In conclusion, the k dependence to the SC gap function comes from the nearest neighbour attractive potential, as can be seen from equation (2.17), results in producing the correct $d-$wave quasiparticle DOS spectrum as observed in experiments. Different configurations of correlation functions $\{\Delta_x^{\pm}, \Delta_y^{\pm}\}$ give us different unconventional superconducting orders which we will soon see become stable self-consistent solutions. We also checked the spectrum of the Hamiltonian and confirm the $E/-E$ symmetry due to redundancy.

3.2 Spin-dependent disorder

In this section, we reproduce the results by Nanguneri et. al. (Nanguneri et al., 2012) using the real space calculations introduced earlier. The model used in this work is slightly different from the one in previous section - the nearest neighbour interaction is absent. Only on-site attractive potential is considered therefore, this corresponds to working with only conventional $s-$wave order. As we discussed earlier, an $s-$wave superconductor is robust against disorder, however the story changes if we consider *spin-dependent* disorder. In (Nanguneri et al., 2012), they have considered two kinds of *spin-dependent* disorder - on-site disorder and hopping disorder - and showed that energy gap and averaged $s-$wave order parameter vanish, unlike the case of spin-symmetric disorder, at some critical value of disorder strength. They also showed that energy gap vanishes first which leads to existence of a gap-less superconducting state. In this section,

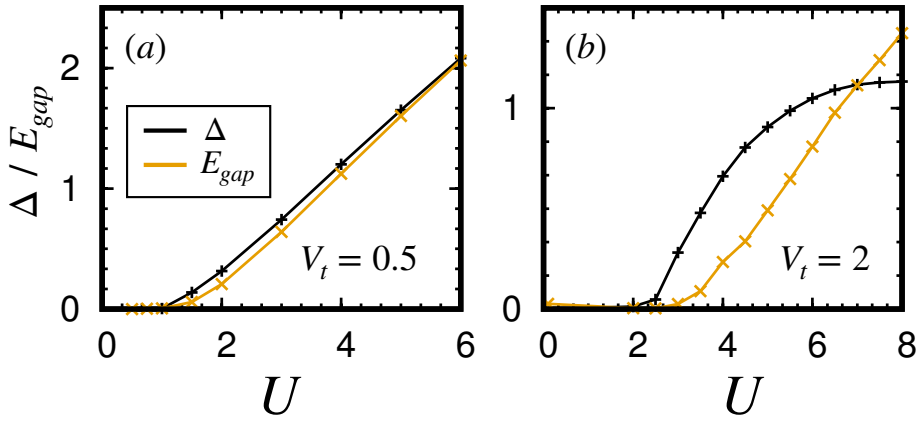

Figure 3.2.2: E_{gap} and Δ variation with on-site interaction U at different disorder strengths.

we do a similar analysis and confirm their reports. Qualitatively the phase diagrams are similar for both kinds of disorder so we only show plots with hopping disorder. The superconducting order parameter Δ is defined as $\Delta = -U\langle c_{i\downarrow} c_{i\uparrow}\rangle$ and the energy gap E_{gap} is the first excited state above the chemical potential. All calculations are performed on a two dimensional attractive Hubbard model of size 24×24. Figure 3.2.1 shows E_{gap} and Δ variation with temperature at different disorder strengths at fixed $U = -2$. Clearly, the SC order parameter Δ is more robust against disorder than the energy gap which suggests that at some critical disorder strength, a gapless superconducting state exists where $\Delta \neq 0$ and $E_{\text{gap}} = 0$. Once the superconducting order parameter Δ is destroyed, the energy gap again become non-zero and increases. This reflects the fact that since there is no superconducting order remaining locally Anderson insulating state takes over. Also notice that the critical temperature of transition is lowered significantly as the disorder strength is increased. It is however not necessary that the energy gap E_{gap} is always less than the SC order parameter Δ. Figure 3.2.2 shows that for low disorder $V_t = 0.5$, as on-site attractive potential is increased, the energy gap and the SC order parameter increases without bound and $E_{\text{gap}} < \Delta$ always. However, at higher disorder strength $V_t = 2.0$, the SC order parameter converges with increasing U and the energy gap increases without bound. This results in energy gap becoming greater than SC order parameter at some U. Next we present a two-dimensional $V_t - T$ phase diagram. Figure 3.2.3 shows the different phases - Gapped superconductor (SC), Gapless superconductor, and Anderson Insulator. The on-site potential was kept at $U = -2$ and the average particle density was maintained at $\langle n\rangle = 0.875$ for this phase diagram.

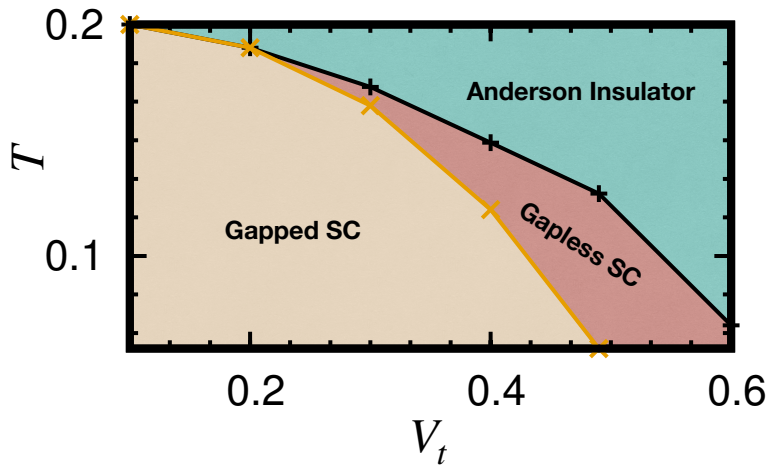

Figure 3.2.3: $V_t - T$ phase diagram showing gapped SC, gapless SC, and Anderson insulating phases.

The phase diagram with on-site spin-dependent disorder is qualitatively similar to the one shown here. The gapless SC phase has lowest-lying quasiparticle excitation energy to be zero. This suggests that in the Gapless SC state, there are islands of Anderson insulating and superconducting states and these gapless states lie in the Anderson insulator region where there is no SC order locally. In conclusion, we confirm the reports by Nanguneri *et. al.* in (Nanguneri et al., 2012) by explicitly matching every plot in their article by our calculations.

3.3 $(-U, -V)$ monolayer model

In this section we work with uniform system and include nearest neighbour interaction term to incorporate unconventional superconductivity. Fourier transforming nearest neighbour interaction term brings in the $k-$dependence to the SC order parameter via equation (2.17). It is thus believed that nearest neighbour attraction favours the formation of a Cooper pair with a large amplitude of the wave function at non-zero distances, rather than at the origin which is the case for on-site attraction. This is achieved by the electrons in the pair having finite relative orbital angular momentum which gives rise to unconventional superconductivity. Strong on-site Coulombic repulsion may also favour formation of Cooper pair with large amplitude therefore it is for that reason sometimes unconventional superconductivity is also thought be a phenomenon of strong correlations. In figure 3.3.1 we show one-dimensional phase diagram showing different self-

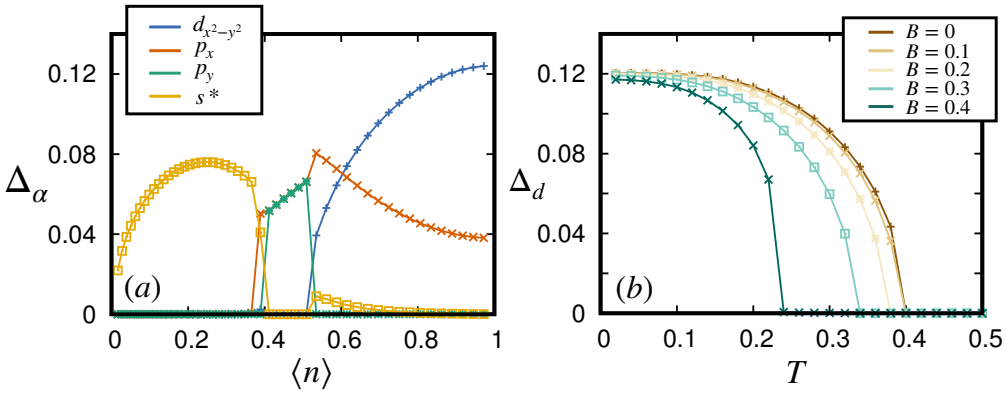

Figure 3.3.1: (a) One-dimensional phase diagram with fixed density, (b) $d$wave SC order variation with temperature in the presence of Zeeman field.

consistent unconventional superconducting orders stable at different particle densities at $T = 0$ and $V = -2.2, U = -1$. The exotic $d + p_x$ mixed phase seem to be stable at densities from 0.6 to 1.0 for all but weak attractive potential. In the case of weaker attractive interaction, $|V| < 2$ only $d-$wave SC order is stable. The two dimensional $U - n$ and $V - n$ phase diagrams, although not shown here, are qualitatively similar to the ones reported in (S. Nayak et al., 2018). The mixed $d + p_x$ phase is particularly interesting because it is a mixed singlet and triplet superconductor! Although, a possible mixing of a $p-$wave component with the $d-$wave order has been inferred via thermal transport measurements (Movshovich et al., 1998) and some theoretical studies (Gor'kov et al., 2001), the understanding of such exotic phases is still lacking.

Lower densities favours the well known $p_x + ip_y$ SC order and extended s (denoted by s^*). Note that due to the presence of attractive interaction U, s^* is always accompanied by the conventional $s$wave order which is not shown here but it is to be remembered that it is always present along with s^*. In plot 3.3.1-(b), we show temperature dependence of $d-$wave order in the presence of Zeeman field, at $V = 2.0$ and $\langle n \rangle = 1.0$. In the presence of higher Zeeman field, which is responsible for asymmetry between up and down spins, critical temperature decreases since the Cooper pair we are considering in our case consists of up-down pairing. It is expected that a Cooper pair with up-up (or down-down) pairing will get more stabilized with increase in Zeeman field.

Next in figure 3.3.2 we show ground state energy variation with the phase difference between mixed SC orders to show the phases we have obtained are indeed the most stable configurations possible. Mixture of only (p_x and p_y) and (d and $s*$) prefers to

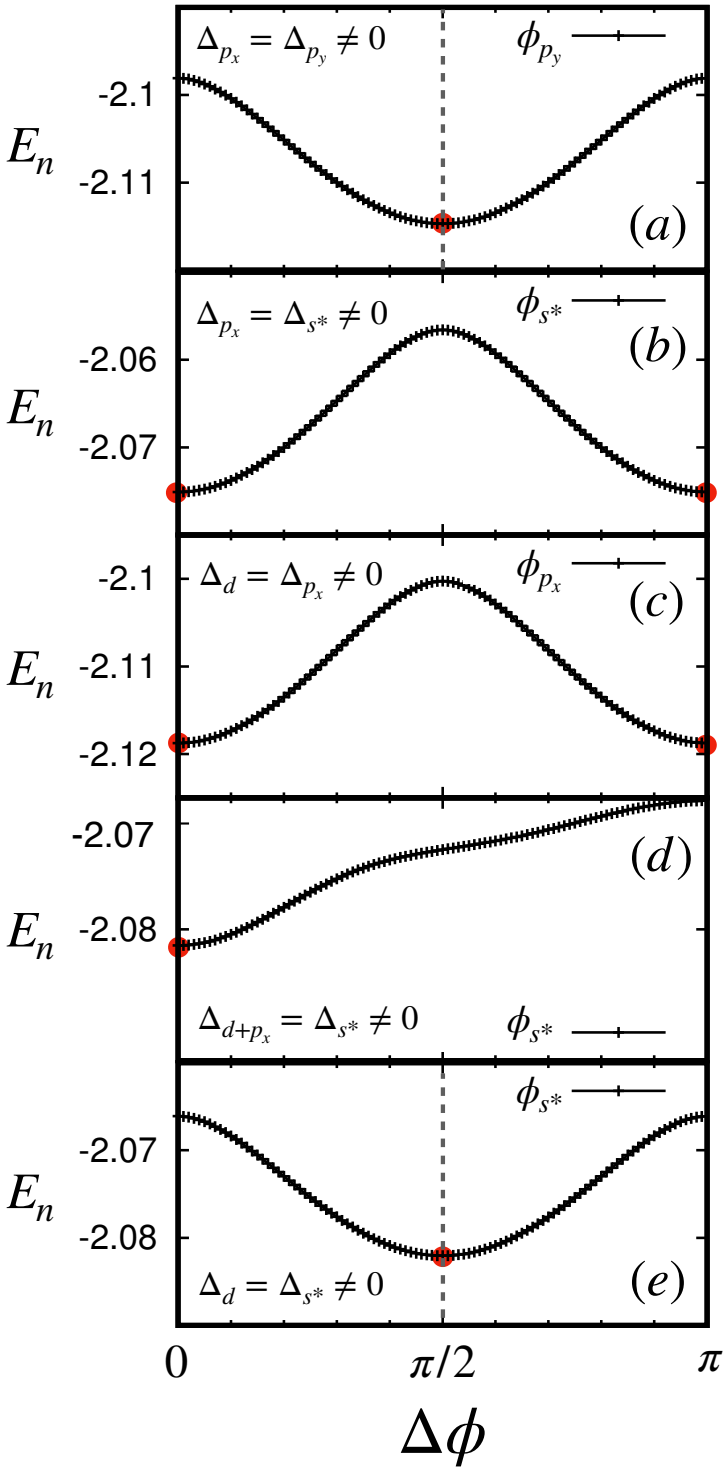

Figure 3.3.2: Energy variation with phase between different mixed SC orders.

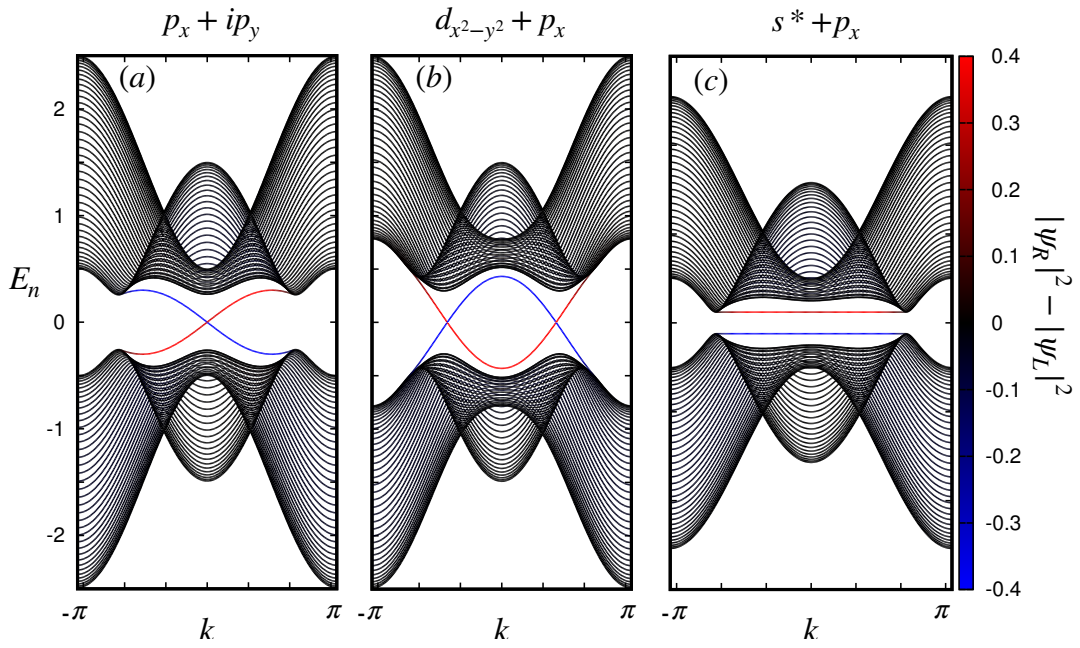

Figure 3.3.3: Band structures of different unconventional SC orders in cylinder geometry.

have a relative phase difference of $\pi/2$ to attain a energetically stable configuration. These agree with the self-consistent SC solutions we have observed in this model.

Now, we would like to topologically classify the SC phases, obtained in 3.3.1, based on their Chern indices, presented earlier in (2.88), and band structures. From the Bulk-boundary correspondence, a Chern number calculated for a Hamiltonian with toric (periodic in x and y direction) boundaries will tell us about the existence of edge modes in one less dimensions which, in our case, is a cylinder geometry. In cylinder geometry, we open the periodic boundaries along one of the directions and keep the other direction periodic - which looks like a cylinder. To solve for this Hamiltonian, we can think of an open chain with N_x orbitals and consider this chain to be periodic with N_y such chains. Note that only one of k_x and k_y is a good quantum number in the cylinder geometry. Fourier transforming this model will lead to a $2N_x \times 2N_x$ matrix which gives the band structure as shown in figure 3.3.3 for different SC orders. The colorline shows the wavefunction weight on either side of the cylinder indicating which band is responsible for a wavefunction concentrated at the edge (edge state). Clearly, $p_x + ip_y$ SC order has a band crossing which may be due to non-zero Chern number. An intriguing situation occurs for $d_{x^2-y^2} + p_x$ order where band crossings in the gap suggests a

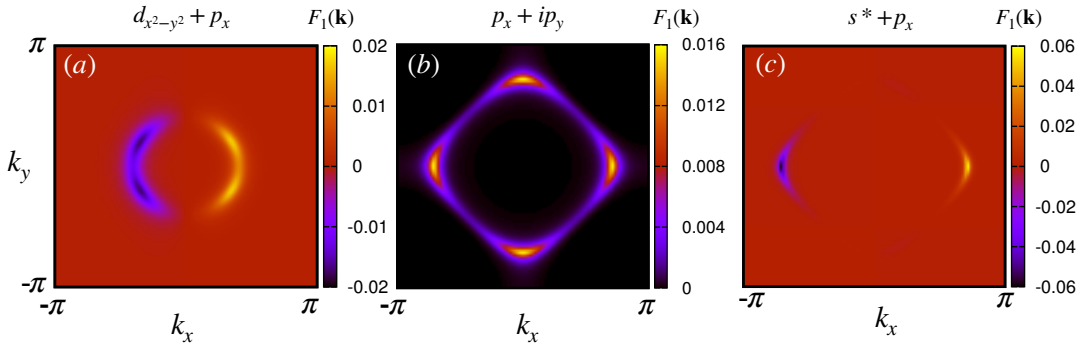

Figure 3.3.4: Local Berry curvature for (a) $d_{x^2-y^2}+p_x$ (b) p_x+ip_y and (c) $s*+p_x$ order.

pair of states are present on each edge, while the topology of the bulk band will remain trivial in this case as the states traverse back to their respective original band. A similar situation occurs for s^*+p_x order where the bands do not cross but mid gap states exists which have finite support on the edges. The Chern analysis leads to a Chern number of $+1$ for p_x+ip_y SC phase whereas, $d_{x^2-y^2}+p_x$ and s^*+p_x has a Chern number of 0 as expected for all values of the chemical potential μ.

In figure 3.3.4 we show local Berry curvature $F(\mathbf{k})$ calculated using equation (2.87). For orders $d_{x^2-y^2}+p_x$ and $s*+p_x$, locally the Berry curvature has positive values and negative values at various locations in the Brillouin zone. Summing the Berry curvature over the Brillouin zone will cancel these contributions and leads to zero Chern number. The story of p_x+ip_y SC phase is however different. The local Berry phase is only positive therefore there is nothing to cancel the local contributions. Summing over the entire Brillouin zone adds the local contributions and give a Chern number of 1. Notice that these plots are shown at a particular value of μ and thus the shape and values of local Berry curvature change as we vary μ, however the overall feature of local Berry curvature cancellation do not change and hence the Chern Number is insensitive to the chemical potential here. We will soon see that in bilayer systems, the Chern number for p_x+ip_y phase will become chemical potential dependent!

3.4 $(+U,-V)$ monolayer model

Next, we move to a case when the on-site potential is repulsive. For this case, we expect anti-ferromagnetic order to appear when U is large as compared to the nearest

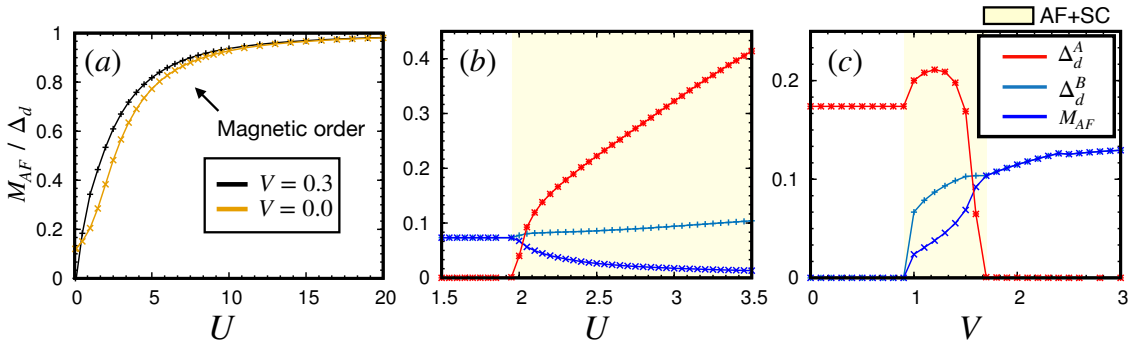

Figure 3.4.1: Coexistence of antiferromagetic and modulated superconducting phase.

neighbour attractive potential V. In figure 3.4.1-(a) we show the AFM order parameter, staggered magnetization M_{AF} variation with increasing on-site repulsive potential. As expected increasing U, which is responsible for the existence of AFM order, enhances the AFM order while SC orders all remain zero until the magnetization saturates. Notice that when $V = 0$, there exists magnetic order even when $U \to 0$; this is due to spontaneous magnetization due to energy minimization. Once V is turned on, spontaneous magnetization do not occur. Also note that at fixed U, magnetization in the presence of V is *more* than the case when $V = 0$! This is due to the Hartree shift (mean field density channel) terms that are present when V is non-zero. The term looks like, $H_I = -V \sum_{ij\sigma} n_{i\sigma} \langle n_{j\bar{\sigma}} \rangle$ which favour AFM order to lower ground state energy.

We now do a self-consistent calculation at varying on-site repulsion U and nearest neighbour attraction V. Figure 3.4.1-(b) shows stable solutions with varying U and at fixed $V = -1$. The calculation was performed in real space formalism with lattice size to be 24×24 and particle density fixed at $\langle n \rangle = 0.875$ We expect for large U, AFM order to dominate. Interestingly, we observe coexistence of AF and SC order as U increases! It is also very interesting that we could find only coexistence of $d-$wave order with AFM. In the case of AF+SC coexisting phase, when we look at the local superconducting order we see a non-uniform feature - the SC order forms alternate patterns of high and low SC order parameter very much like an AFM staggered magnetic order. This non-uniform modulated structure exists only in the presence of an AFM phase. This SC modulation is a special case of *pair density wave* of (π, π) ordering in $d-$wave superconductor. The unit cell is doubled in (π, π) ordering and the two sublattice sites are labelled as site A and site B, which correspond to their respective SC order parameter $\Delta_d^{A/B}$ in figure 3.4.1(b)-(c). From plot (b), we observe that the SC order is uniform

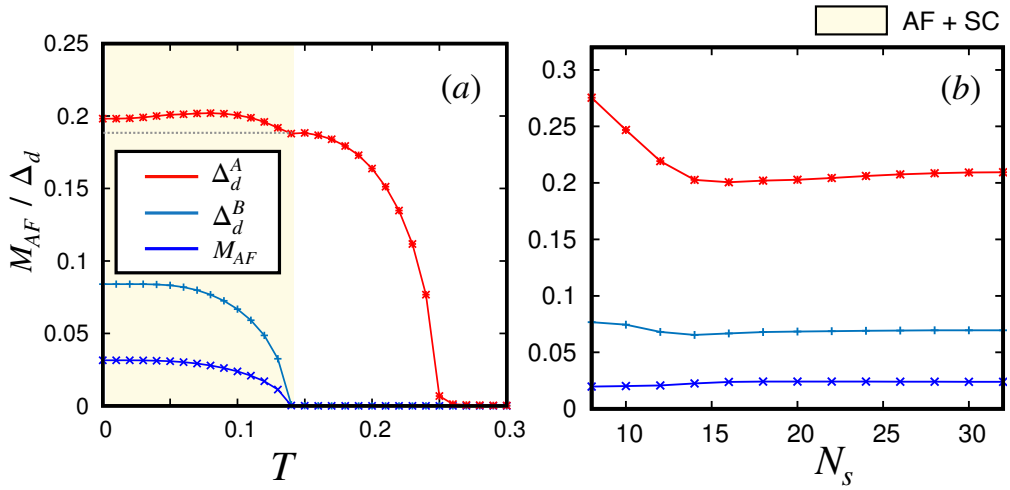

Figure 3.4.2: (a) Temperature variation of AF+SC phase (b) Order fluctuation as lattice size N_s is changed.

when, U is small enough that no AFM order is present. Once U becomes large, the two sites attain different SC orders - as long as the AFM phase becomes more enhanced with increasing U, the difference $|\Delta_d^A| - |\Delta_d^B|$ for two sub-lattice sites also increases. In figure 3.4.1-(c) we show order parameter variation with V at fixed $U = 2.5$. Here again we see that site A and site B attains different SC order parameter when $d-$wave order coexists with AFM. Large V limit is where pure $d-$wave (uniform) superconductor exists. Only when $V \approx U$ then the AF+SC (π, π) pair density wave exists. Further increasing V results in a mixed $d + p$ phase. We now look at temperature variation of this AF+SC coexisting phase.

Figure 3.4.2-(a) shows the temperature variation. We see that with increasing temperature the SC order is destroyed first, this transition from AF+SC phase to a purely AFM phase changes the trajectory (variation) with temperature with a kink and finally the magnetic order goes to zero. If we were to extrapolate the magnetic order, at say $T = 0.2$, to a saturated zero temperature magnetic order, we will end up with a slightly lesser value than what it actually attains. This suggests that the anti-ferro order gets enhanced by the co-existence of (π, π) modulated $d-$wave superconducting order. This same behaviour is also observed with Zeeman field variation. This may be a hint that the AFM in the presence of the SC phase behaves slightly differently when only the AF phase is present. Which supports the statement that SC+AF phase is really a new order rather than just being a mixed order! Now since we are working in real space formal-

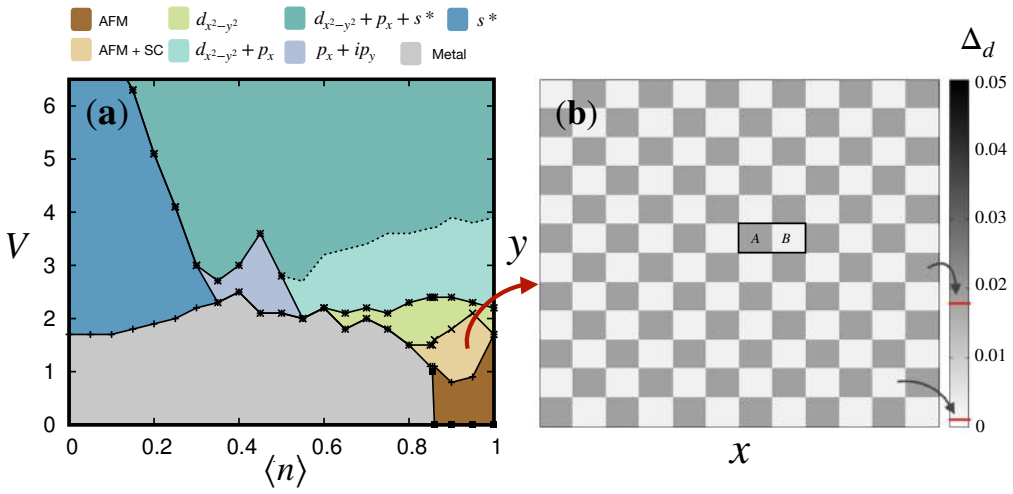

Figure 3.4.3: (a) $V - \langle n \rangle$ phase diagram for (+U,-V) model, (b) (π, π) pair density wave order in $d-$wave superconductor due to coexistence with AFM

ism, being limited by computational power that all these calculations were performed on a lattice size of 24×24. We therefore ask whether this behaviour is a consequence of finite size. To prove that the AF+SC phase is stable with lattice size we run the simulation for different lattice sizes as shown in figure 3.4.2-(b). There are fluctuations for lattice sizes below 15 however, the solution seem to converge for higher lattice sizes therefore we can say the existence of AF+SC order is not a manifestation of some finite size effect.

Next we show a two dimensional $V - n$ phase diagram with all the exotic phases, see figure 3.4.3-(a). This diagram was plotted at $T = 0$ and $U = 2.5$. Notice that the phase diagram is qualitatively similar to the phase diagram for $(-U, -V)$ model expect for the fact below a value of $V \approx 2$, metallic phase exists at densities away from half-filling and near half-filling AFM exists. This can be understood as in $(+U, -V)$ model, there is a completion between on-site repulsion and nearest neighbour attraction therefore below a threshold V the phase diagram is due to on-site repulsion and above that limit attractive interaction dominates and hence the phase diagram is similar to the one for $(-U, -V)$ model.

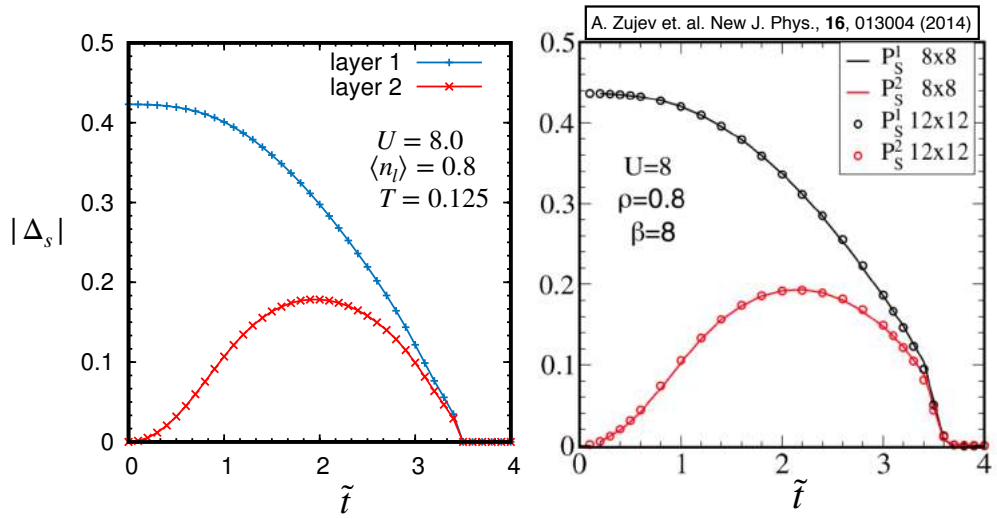

Figure 3.5.1: (a) Layer-wise SC order parameter for the given starting configuration vs interlayer tunneling (b) proximity induced SC reported in (Zujev et al., 2014).

3.5 $(-U, -V)$ bilayer model and proximity effect

After understanding the phase diagrams in monolayer models we now introduce a metallic tight binding layer in proximity to the first. We do this by introducing a new parameter, $\tilde{t}$, that couples the two layers by allowing interlayer tunnelling. We label the SC layer which has $(-U, -V)$ interactions present as layer 1 ($l = 1$) and a metallic layer which is just a tight binding model as layer 2 ($l = 2$). The Bogoliubov-de Gennes equations for this model are derived in section 2.2. Allowing the electrons to tunnel between the two layers naturally gives rise to proximity effect since the Cooper pairs will now have non-zero amplitudes in the metallic layer due to tunnelling. This forces the metallic layer to attain non-zero pair correlations which will be a signature of induced SC we will look for. These correlations are calculated similar to the self-consistent correlations for the SC layer but they are not fed back into the Hamiltonian as self-consistency is performed. Only the pair correlations for SC layer enter the Hamiltonian for self-consistency. To test this, we first perform checks in the limit $\tilde{t} = 0$, which decouples the two layers, and we obtain the monolayer results and also the pair correlations in layer 2 are zero. By plotting the density of states for layer 2 in this limit resulted in a metallic DOS with van hove singularity as is expected. Then we slowly turn on the interlayer coupling $\tilde{t}$ and monitor what happens to the pair correlations in both the layers. Figure 3.5.1 shows the $s-$wave order parameter for layer 1 (SC) and layer 2 (metal)

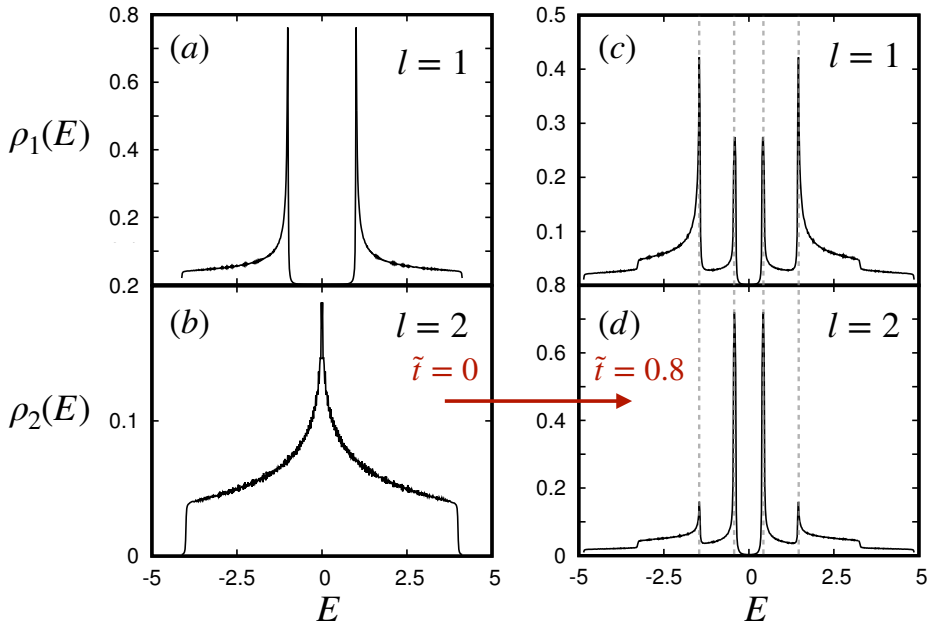

Figure 3.5.2: Density of states for SC and metallic layer as interlayer tunnelling is switched on.

as interlayer tunnelling is increased. To compare our results with previously reported results we also show a plot 3.5.1-(b) taken from (Zujev et al., 2014). The induced (in metallic layer) pairing correlations becomes non-zero as $\tilde{t}$ is turned on, meanwhile the pairing correlations in the superconducting layer decreases. This decrease is natural since Cooper pairs now have non-zero support in layer 2 and consequently lesser support in layer 1. As $\tilde{t}$ is further increased, the SC in both the layers is eventually killed. One immediate thing to notice is that the critical value of tunnelling is the same for both the layers. This makes sense because the energy gained from attractive interaction is now overcome by the energy gained from interlayer tunnelling. This is further checked by increasing the attractive potential in layer 1 increases the critical value of interlayer tunnelling. We now define layer-wise density of states,

$$\rho_{i\sigma l}(E) = \sum_n \left(|u_{i\sigma}^{ln}|^2 d_\gamma(E_n - E) + |v_{i\sigma}^{ln}|^2 d_\gamma(E_n + E) \right) \tag{3.1}$$

where $d_\gamma(E_n - E) = \frac{\gamma/\pi}{\gamma^2 + (E - E_i)^2}$. This definition is a generalization of the previous definition where instead of just doing a sum, we do a weighted sum using the wave function amplitude to get the local site-wise density of state and then we do a layer

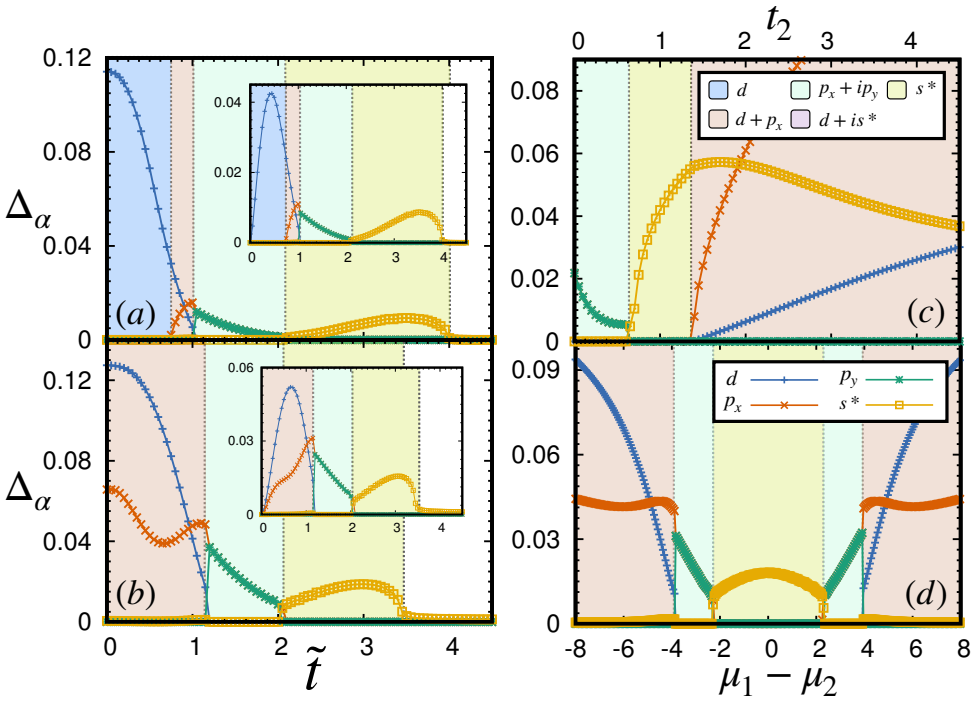

Figure 3.5.3: SC order transitions induced by tunnelling $\tilde{t}$, bandwith of the metallic layer t_2, and gate voltage $\mu_1 - \mu_2$.

average of $\rho_{i\sigma l}(E)$ to get the layer-wise density of states,

$$\rho_l(E) = \sum_{i\sigma \in l} \rho_{i\sigma l}(E) \qquad l \in \{1, 2\} \tag{3.2}$$

Let us now look at the density of states in the induced layer to get some information about the nature of the induced superconducting order. In figure 3.5.2 we show how interlayer tunnelling alters the density of states of the two layer. Plots (a) and (b) show the DOS for layer 1 and 2 respectively for the case when $\tilde{t} = 0$. In this limit the two layers are decoupled and therefore we obtain, in layer 1, the usual $s-$wave SC gap and, in layer 2, the two dimensional tight binding DOS. As $\tilde{t}$ is switched on, both layers become gapped and have two pairs of coherence peaks each. These pairs of coherence peaks portray the fact that there are two different superconducting gaps present. It is very interesting since existence of such multiple pairs of coherence peaks is sometimes referred to as a signature of mixed superconducting order but in this case it is really just a *feedback* from the proximity effect that shows this behaviour.

We now show that interlayer tunnelling can bring about transitions in superconduct-

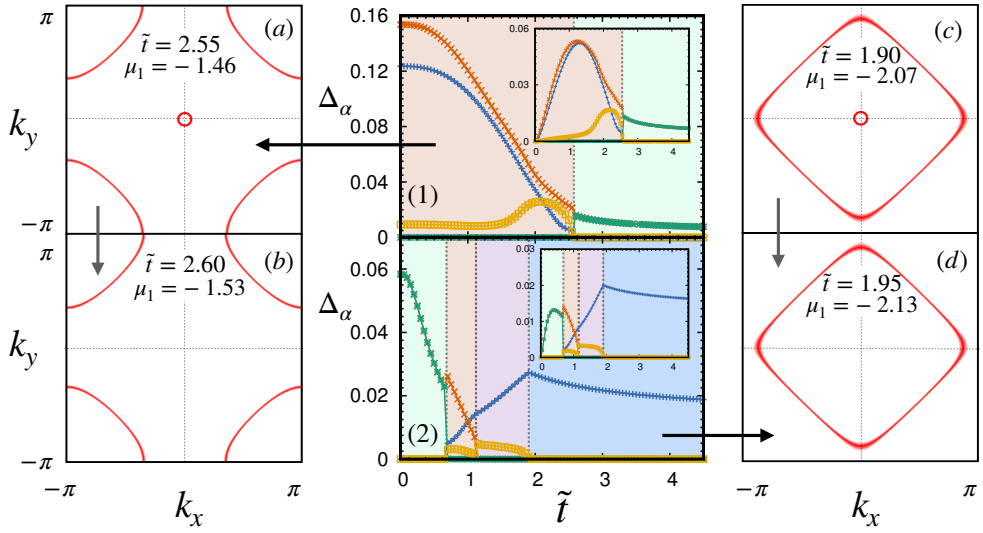

Figure 3.5.4: Connection of superconducting transitions to Lifshitz transitions in the non-interacting model.

ing order. Not only interlayer tunnelling, these transitions can also be controlled by experimentally viable control parameters, the bandwidth of the metallic layer and the gate potential. Figure 3.5.3 show such transitions. In plots (a) and (b) starting with some initial configuration in our the parameter space, we start increasing interlayer tunnelling $\tilde{t}$. At first the usual proximity effect behaviour is observed as was observed in figure 3.5.1. On further increasing $\tilde{t}$, $p_x + ip_y$ order becomes non-zero whereas d (or $d + p_x$) goes to zero. Then again a transition occurs to s^* on further increasing $\tilde{t}$ after which superconductivity finally is killed. The second layer just mirrors the phases that appear in layer 1 and can be seen from the insets in figure 3.5.3-(a-b). Such transitions are also observed when the bandwidth of the metallic layer t_2 is changed figure 3.5.3-(c) and with gate potential $\mu_1 - \mu_2$ also, 3.5.3-(d). These simulations were performed while keeping the densities in each layer fixed and equal except for the plot (d). However, this was also checked when this fixed density restriction was relaxed - the one-dimensional phase diagrams are qualitatively similar to the ones shown. We would like to emphasis that this feature rules out the possibility that superconducting transitions reported here can simply be a consequence of effective density change in layer 1. In figure 3.5.4 we show that some of the superconducting transitions correlate perfectly with *Lifshitz transitions* in the corresponding non-interacting ($U = V = 0$) model. Lifshitz transitions are transitions of the topology of the Fermi surface and these transitions are known to give rise to anomalies in the electron characteristics of metals

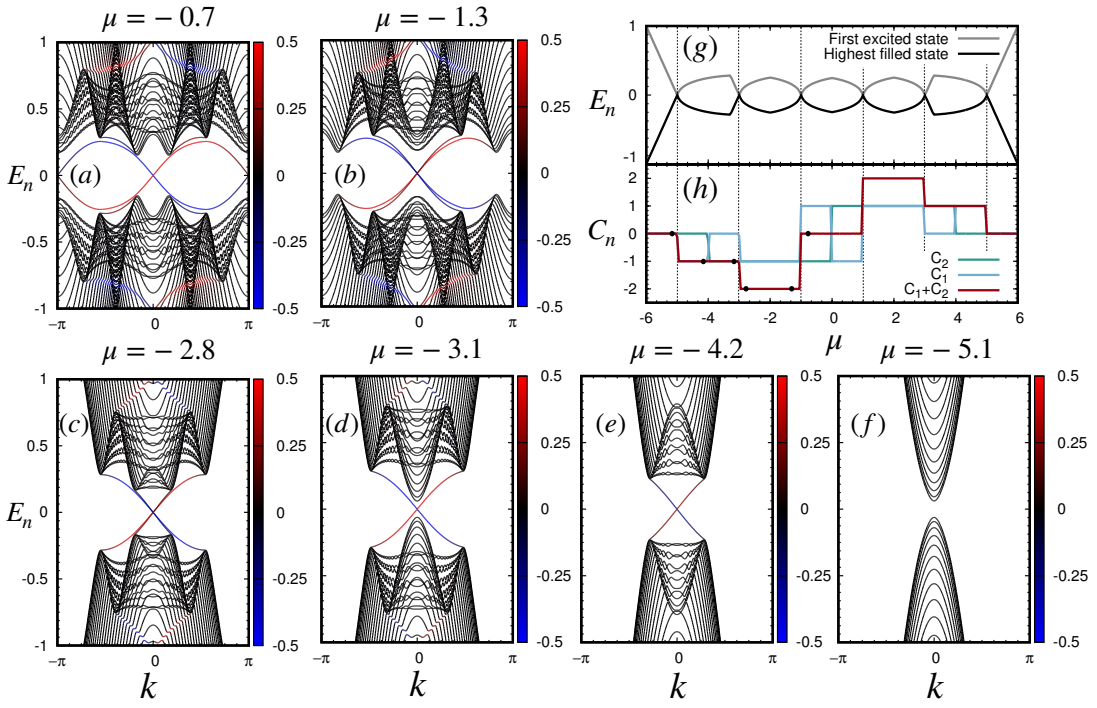

Figure 3.5.5: Band structure of $p_x + ip_y$ and its variation with chemical potential μ in bilayer model calculated in cylinder geometry.

(Volovik, 2017). Figure 3.5.4-(1) corresponds to (a) and (b) while (2) corresponds to (c) and (d). The non-interacting Fermi surfaces show a qualitative change as the superconducting order changes abruptly. The electron-like Fermi pocket near $k = 0$ disappears and therefore, one of the non-interacting bands stops contributing to pairing. This background Lifshitz transitions changes the topology of the Bogoliubov quasi-particle bands which induces a topological superconducting transition. Note that this correspondence is not found for all such transitions.

Next we characterize the non-trivial $p_x + ip_y$ phase in terms of edge-state spectra and Chern indices as we did for the monolayer case. First we analyze Berry curvature and compute topological invariants, Chern numbers, associated with each quasiparticle band (since we now have two filled bands at $T = 0$). Interestingly, the topological character of a SC state changes with the chemical potential μ ($= \mu_1 = \mu_2$). In figure 3.5.5-(g-h) we show the SC gap as a function of chemical potential. The gap closes and reopens upon varying μ. Each such gap closing is associated with a change in the *total* topological invariant, $C_1 + C_2$ of the bands. We also compute the edge-state spectra by imposing open boundary conditions in one of the directions, leading to cylinder

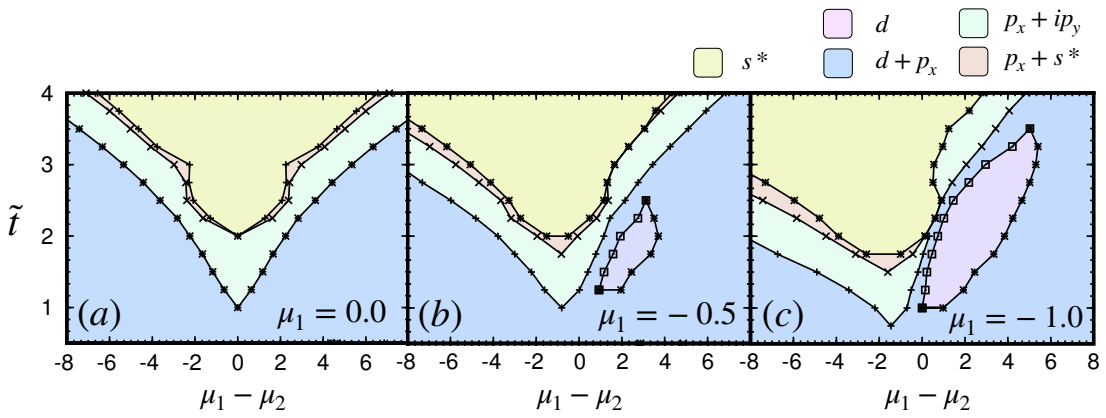

Figure 3.5.6: $\tilde{t} - (\mu_1 - \mu_2)$ phase diagram at $T = 0$ and $U = 1, V = 2.5$ for bilayer model.

geometry, and plotting the tower of states as a function of k_x or k_y. Figure 3.5.5-(a-f) show the Band structure for representative values of μ corresponding to the black dots marked on the Chern number plots. The color code on the energy eigenvalues represents the difference of the weight on left and that on right edges of the corresponding state. From plots (a) to (b) two states cross the bulk gap, however the gap is crossed twice which is reflected in the change in Chern number from 0 to -2. Notice for (a), although both bands have a non-zero Chern number, the total Chern index is zero. From $\mu = -2.8$ to $\mu = -3.1$, one of the bands pulls away and only one pair of edge states remain and correspondingly, Chern number for one of the bands become zero (Batra et al., 2019). Finally, from $\mu = -4.2$ to $\mu = -5.1$ another pair of edge states pull away and the total Chern number becomes zero. Finally, in figure 3.4.3 we show $\tilde{t} - (\mu_1 - \mu_2)$ phase diagram at $T = 0$ and $U = 1, V = 2.5$. Notice how at non-zero μ_1, asymmetry is present whereas for $\mu_1 = 0$, the phase diagram is symmetric about $\mu_1 - \mu_2$. As μ_1 is changed from 0, an island of $d-$wave region appears and extends in size. Also the $p_x + s^*$ order is seen to be stable only on one of the sides of the diagram as μ_1 moves away form zero.

Finally, I would like to end this chapter by reminding that insights from our results on a simple model for proximity induced superconductivity may open up a new route to discover topological superconductors.

Chapter 4

Concluding Remarks

We first summarize some of the results we discussed in the previous chapter - after developing the models and methods we first performed some consistency checks in order to obtain what we already know about superconductivity. This involved studying the density of state (DOS) spectra for various superconducting phases and comparing them to experimentally measured DOS via STM. Switching on superconductivity opens a gap at the Fermi energy (in our case zero energy) which corresponds to the van Hove's singularity point (since our non interacting model is 2D metallic) ref. 3.1.1. In the conventional case we obtain the gap being equal to the difference between the two coherence peaks which indeed was equal to $2\Delta_{\text{op}}$ ref. 3.1.2(a). For the unconventional case this is not always true - in the case of $d-$wave order the gap is always zero (ref 3.1.2(b))! After that we did some checks on the symmetry property of the BdG method due to redundancy - the spectrum obtained from the two blocks of the 4×4 Hamiltonian was checked. We obtained that the two spectra (eigenvalue and eigenvectors) matched (with appropriate transformation) with the error being in the 7^{th} decimal place that is interpreted to be a numerical error ref. 3.1.3(a). We also checked whether self-consistent method is equivalent to energy minimization by varying different order parameters and calculating their ground state energies ref. 2.1.3. Verification of the code was also performed by reproducing the results in (Nanguneri et al., 2012) in which the interplay of spin-dependent disorder and superconductivity was studied. It was found that the energy gap, which was defined as the first excited state above the chemical potential, and the superconducting order parameter vanish at different disorder strengths leading to a gapless superconducting state. All the results claimed in (Nanguneri et al., 2012) were reproduced within the numerical error.

Next we showed how nearest neighbour interaction strength supports unconventional (sometimes mixed) superconducting phases ref. 3.3.1. We also performed Chern number calculations and characterized these phases based on their Chern indices and found $p_x + ip_y$ as topologically non-trivial. This claim was further tested by looking at their band structures in one lesser dimensions which did result in band crossing ref. 3.3.3 - these states corresponded to edge states. Band crossings were also observed in $d + p_x$ phase but those states traverse back to the original band - this may have links to Berry curvature being locally non-zero (ref. 3.3.4) but on summing over the entire Brillouin zone, resulted in zero Chern index. Although we may be tempted to call $d+p_x$ phase topologically trivial but as shown in a recent work (F. Liu et al., 2017), we can have topologically non-trivial phases with zero Berry curvature. The existence of edge states in $d + p_x$ SC state puts us in doubt. It is shown in (F. Liu et al., 2017) that the topological invariants are not calculated from Berry curvature, since it turns out to be zero. Instead, Berry connection whose integration over the momentum space, the so-called 2D Zak phase (Zak, 1989) provides the topological invariant for such a system. Therefore the topological classification of $d + p_x$ is unclear.

We then introduced on-site *repulsive* interaction that supports AFM order - this allowed us to study the competition between superconductivity and anti-feromagnetism. Interestingly, we found a region where both these phase coexisted ref. 3.4.3(a). On further exploration, if was found that due to their coexistence, the AFM order gets enhanced 3.4.1,3.4.2. The local SC pairing correlation variation revealed the (π, π) pair density modulation 3.4.3(b). This presents us with a problem of defining the order parameter from the correlation function. Since now two adjacent bond-links on the lattice attain different pair correlations, we need to figure out how to define the triplet component. For example, to define, say p_x order, there are two ways,

$$\Delta^i_{p_x} \stackrel{?}{=} \langle c_{i+x\downarrow} c_{i\uparrow} \rangle - \langle c_{i-x\downarrow} c_{i\uparrow} \rangle \tag{4.1}$$

and

$$\Delta^i_{p_x} \stackrel{?}{=} \langle c_{i+x\downarrow} c_{i\uparrow} \rangle - \langle c_{i\downarrow} c_{i+x\uparrow} \rangle \tag{4.2}$$

This ambiguity in defining the order parameters needs to be sorted out before we go ahead and claim a phase to be whether of $d-$wave type or $p-$wave type. Once this ambiguity is resolved, a momentum space calculation for this model can be set up with the lattice allowing (π, π) ordering which will further add to the complexity of

our calculations. Also, there is a problem of mean field approximation that we have made throughout our calculations. Mean field approach do not capture the physics arising due to quantum fluctuations. They become necessary close to the phase boundary where quantum fluctuations become large and cannot be neglected. In previous reports (Abram et al., 2013), they have shown how these anti-ferro and superconducting coexisting phase may be a consequence of approximation. The exact calculations, which of course is very tedious to do due to its extremely large Hilbert space, may not have such coexisting phases. Although a possible mixing of a $p-$wave component with the $d-$wave order has been inferred via thermal transport measurements (Movshovich et al., 1998) and some theoretical studies (Gor'kov et al., 2001); this question of going beyond mean field approach is relevant even in the $(-U, -V)$ model where the stability of the mixed singlet and triplet superconducting phase, $d + p_x$ needs to be checked.

We then studied proximity effect by coupling the 2D EAHM with the tight-binding model via interlayer tunnelling. We showed that such a prototype model of proximity induced superconductivity displays transitions between topologically trivial and non-trivial SC states ref. 3.5.3. It is worthwhile to note that a general treatment of the superconducting pairing correlations, as previously carried out in (S. Nayak et al., 2018), which allows for various broken symmetry order parameters (singlet or triplet) is important to obtain the non-trivial topological transitions. In defining the model, we do not impose any symmetry constraints on the correlation function expect for the fact that they need to be uniform in order to be considered in momentum space. This uniform condition rules out the possibility of any kind of pair density wave or, in general, Fulde-Ferrell-Larkin-Ovchinnikov[1] (FFLO) type of order to exist. This is worth mentioning since we witnessed such states in section 3.4. On the whole, the general treatment considered in the work compares energies of different superconducting broken symmetry phases and selects the one most stable for a given configuration. It is also worth noting that since we work in discrete space, we have defined our order parameters according to those finitely many discrete points[2]. A natural extension to this work would be to allow of all components of triplet pairing, $\uparrow\uparrow$ and $\downarrow\downarrow$, the ones we neglected in the beginning. Since these pairings will result in a triplet superconductor, we expect them to be relevant where either $p_x + ip_y$ SC phase is stable or $d + p_x$ singlet-triplet mixed phase is

[1] One of the characteristics of FFLO state is that the Cooper pairs have non-zero total momentum ($\langle c_{-k+q\downarrow} c_{k\uparrow} \rangle \neq 0$) and a spatially non-uniform order parameter.

[2] The true symmetry properties of the correlation functions can be known *only* in continuum

stable. An important question after allowing all triplet pairings would be the effect of Magnetic field on superconductivity - since Zeeman field break the ↑-spin and ↓-spin degeneracy, we expect a competition within the triplet superconductivity in the presence of magnetic field. Finally, the results presented in section 3.5 are directly relevant to systems that exhibit superconductivity in atomically thin layers, such as monolayers of CuO_2 (G.-Y. Zhu et al., 2016) and bilayer graphene (Cao et al., 2018).

Although a microscopic theory of unconventional superconductivity is still awaited, the models considered in this thesis can serve as an effective description of many unconventional superconductors. In the end, I would like to say that it is probably not an exaggeration to say that the field of superconductivity remains as young as it was a hundred years ago, being able to constantly surprise and fascinate even the most experienced researchers.

Bibliography

Abram, M. et al. (2013). "d-wave superconductivity and its coexistence with antiferromagnetism in the $t - J - U$ model: Statistically consistent Gutzwiller approach". In: *Physical Review B,* **88**, 094502.

Aggarwal, Leena et al. (2016). "Unconventional superconductivity at mesoscopic point contacts on the 3D Dirac semimetal Cd_3As_2". In: *Nature Materials,* **15**, 1.

Alsharari, Abdulrhman M., Mahmoud M. Asmar, and Sergio E. Ulloa (2018). "Proximity-induced topological phases in bilayer graphene". In: *Physical Review B,* **97**, 241104(R).

Asbóth, János K., László Oroszlány, and András Pályi (2016). *A Short Course on Topological Insulators*. Springer International Publishing.

Ashcroft, Neil W. and N. David Mermin (1976). *Solid State Physics*. Holt, Rinehart and Winston.

Batra, Navketan, Swagatam Nayak, and Sanjeev Kumar (2019). "Topological Transitions in a Model for Proximity Induced Superconductivity". In: *ArXiv: 1902.02532,*

Benalcazar, Wladimir A., B. Andrei Bernevig, and Taylor L. Hughes (2017a). "Electric multipole moments, topological multipole moment pumping, and chiral hinge states in crystalline insulators". In: *Physical Review B,* **96**, 245115.

— (2017b). "Quantized electric multipole insulators". In: *Science,* **357**, 61.

Bernevig, B. Andrei and Taylor L. Hughes (2013). *Topological Insulators and Topological Superconductors*. Princeton University Press.

Cao, Yuan et al. (2018). "Unconventional superconductivity in magic-angle graphene superlattices". In: *Nature,* **556**, 43.

Chen, Chun et al. (2010). "Enhanced superconducting proximity effect in strongly correlated heterostructures". In: *Physical Review B,* **82**, 174502.

Chu, C. W. et al. (1987). "Evidence for Superconductivity above 40 K in the La-Ba-Cu-O Compound System". In: *Physical Review Letters,* **58**, 405.

Dobrosavljevic, Vladimir, Nandini Trivedi, and Jr. James M. Valles (2012). *Conductor-Insulator Quantum Phase Transitions*. Oxford University Press. Chap. 17, Theoretical Studies of Superconductor-Insulator Transitions.

Fukui, Takahiro, Yasuhiro Hatsugai, and Hiroshi Suzuki (2005). "Chern Numbers in Discretized Brillouin Zone: Efficient Method of Computing (Spin) Hall Conductances". In: *Journal of the Physical Society of Japan,* **74**, 6.

Gastiasoro, Maria N. and Brian M. Andersen (2018). "Enhancing superconductivity by disorder". In: *Physical Review B,* **98**, 184510.

Gennes, P. G. De (1999). *Superconductivity Of Metals And Alloys*. Perseus Books.

Gor'kov, Lev P. and Emmanuel I. Rashba (2001). "Superconducting 2D System with Lifted Spin Degeneracy: Mixed Singlet-Triplet State," in: *Physical Review Letters* **87**, 037004.

Hasan, M. Z. and C. L. Kane (2010). "Colloquium: Topological insulators". In: *Reviews of Modern Physics,* **82**.

Ibach, Harald and Hans Luth (2009). *Solid-State Physics*. Springer Berlin Heidelberg.

Kotliar, Gabriel and Jialin Liu (1988). "Superexchange mechanism and d-wave superconductivity," in: *Physical Review B* **38**, 5142(R).

Kruthoff, Jorrit et al. (2017). "Topological Classification of Crystalline Insulators through Band Structure Combinatorics". In: *Physical Review X,* **7**, 041069.

Kumar, Sanjeev and Prabuddha B. Chakraborty (2015). "Suppression of s-wave superconductivity by kinetic disorder in a two-dimensional attractive Hubbard model". In: *The European Physical Journal B,* **88**, 69.

Liu, Feng and Katsunori Wakabayashi (2017). "Novel Topological Phase with a Zero Berry Curvature". In: *Physical Review Letters,* **118**, 076803.

Liu, Xin, J. K. Jain, and Chao-Xing Liu (2014). "Long-Range Spin-Triplet Helix in Proximity Induced Superconductivity in Spin-Orbit-Coupled Systems". In: *Physical Review Letters,* **113**, 227002.

Mackenzie, Andrew Peter and Yoshiteru Maeno (2003). "The superconductivity of Sr_2RuO_4 and the physics of spin-triplet pairing". In: *Reviews of Modern Physics,* **75**.

Monthoux, P., D. Pines, and G. G. Lonzarich (2007). "Superconductivity without phonons," in: *Nature Reviews* **450**, 20/27.

Moore, Joel E. (2010). "The birth of topological insulators". In: *Nature,* **464**, 11.

Movshovich, R. et al. (1998). "Low-Temperature Anomaly in Thermal Conductivity of $Bi_2Sr_2Ca(Cu_{1-x}Ni_x)_2O_8$: Second Superconducting Phase?," in: *Physical Review Letters* **80**, 1968.

Nadj-Perge, Stevan et al. (2008). "Observation of Majorana fermions in ferromagnetic atomic chains on a superconductor". In: *Science,* **346**.

Nanguneri, R. et al. (2012). "Interplay of superconductivity and spin-dependent disorder". In: *Physical Review B,* **85**, 134506.

Nayak, Chetan et al. (2008). "Non-Abelian anyons and topological quantum computation". In: *Reviews of Modern Physics,* **30**.

Nayak, Swagatam and Sanjeev Kumar (2018). "Exotic superconducting states in the extended attractive Hubbard model". In: *Journal of Physics: Condensed Matter,* **30**, 135601.

Oreg, Yuval, Gil Refael, and Felix von Oppen (2010). "Helical Liquids and Majorana Bound States in Quantum Wires". In: *Physical Review Letters,* **105**, 177002.

Potter, Andrew C. and Patrick A. Lee (2011). "Engineering a $p + ip$ superconductor: Comparison of topological insulator and Rashba spin-orbit-coupled materials". In: *Physical Review B,* **83**, 184520.

Qi, Xiao-Liang and Shou-Cheng Zhang (2011). "Topological Insulators and Superconductors". In: *Reviews of Modern Physics,* **83**, 1057.

Reeg, Christopher R. and Dmitrii L. Maslov (2015). "Proximity-induced triplet superconductivity in Rashba materials". In: *Physical Review B,* **92**, 134512.

Sau, Jay D. et al. (2010). "Generic New Platform for Topological Quantum Computation Using Semiconductor Heterostructures". In: *Physical Review Letters,* **104**, 040502.

Shen, Shun-Qing (2017). *Topological Insulators*. Springer Singapore.

Sigrist, Manfred and Kazuo Ueda (1991). "Phenomenological theory of unconventional superconductivity," in: *Reviews of Modern Physics* **63**, 239.

Simon, Steven H. (2013). *The Oxford Solid State Basics*. Oxford University Press.

Thouless, D. J. et al. (1982). "Quantized Hall Conductance in a Two-Dimensional Periodic Potential". In: *Physical Review Letters,* **49**, 6.

Tsuei, C. C. and J. R. Kirtley (2000). "Pairing symmetry in cuprate superconductors". In: *Reviews of Modern Physics,* **72**, 4.

Volovik, G. E. (2017). "Topological Lifshitz Transitions". In: *Low Temperature Physics,* **43**, 1.

Wu, Fengcheng, A. H. MacDonald, and Ivar Martin (2018). "Theory of Phonon-Mediated Superconductivity in Twisted Bilayer Graphene". In: *Physical Review Letters,* **121**, 257001.

Zak, J. (1989). "Berry's Phase for Energy Bands in Solids". In: *Physical Review Letters,* **62**, 23.

Zhang, T. et al. (2010). "Superconductivity in one-atomic-layer metal films grown on Si(111)". In: *Nature Physics,* **6**, 104–108.

Zhu, Guo-Yi, Fu-Chun Zhang, and Guang-Ming Zhang (2016). "Proximity-induced superconductivity in monolayer CuO_2 on cuprate substrates". In: *Physical Review B,* **94**, 174501.

Zhu, Jian-Xin (2016). *Bogoliubov-de Gennes Methods and its Applications*. Springer International Publishing.

Zujev, Aleksander et al. (2014). "Pairing correlations in the two-layer attractive Hubbard model". In: *New Journal of Physics,* **16**, 013004.